

การแก้ไขเลขซีทีที่แปลกปลอมที่เพิ่มขึ้นให้ถูกต้องด้วยอนุพันธ์อันดับสองตามแนวผิวสัมผัส
และการเก็บรักษาเนื้อเยื่ออ่อนสำหรับการล้างลำไส้ใหญ่ในภาพรังสีส่วนตัดอาศัย
คอมพิวเตอร์

นายไกรศร ชุณหงษ์พิพัฒน์

วิทยานิพนธ์นี้เป็นส่วนหนึ่งของการศึกษาตามหลักสูตรปริญญาวิทยาศาสตรดุษฎีบัณฑิต
สาขาวิชาวิทยาการคอมพิวเตอร์และเทคโนโลยีสารสนเทศ
ภาควิชาคณิตศาสตร์และวิทยาการคอมพิวเตอร์
คณะวิทยาศาสตร์ จุฬาลงกรณ์มหาวิทยาลัย
ปีการศึกษา 2559

ลิขสิทธิ์ของจุฬาลงกรณ์มหาวิทยาลัย

บทคัดย่อและแฟ้มข้อมูลฉบับเต็มของวิทยานิพนธ์ตั้งแต่ปีการศึกษา 2554 ที่ให้บริการในคลังปัญญาจุฬาฯ (CUIR)

เป็นแฟ้มข้อมูลของนิสิตเจ้าของวิทยานิพนธ์ที่ส่งผ่านทางบัณฑิตวิทยาลัย

The abstract and full text of theses from the academic year 2011 in Chulalongkorn University Intellectual Repository (CUIR)
are the thesis authors' files submitted through the Graduate School.

GRADIENT DIRECTIONAL SECOND DERIVATIVE PEH CT NUMBER
CORRECTION AND SOFT TISSUE PRESERVATION FOR ELECTRONIC
CLEANSING IN CTC IMAGES

Mr. Krisorn Chunhaponpipat

A Thesis Submitted in Partial Fulfillment of the Requirements
for the Degree of Doctor of Philosophy Program in Computer Science and Information
Technology

Department of Mathematics and Computer Science

Faculty of Science

Chulalongkorn University

Academic Year 2016

Copyright of Chulalongkorn University

Thesis Title GRADIENT DIRECTIONAL SECOND DERIVATIVE PEH CT
NUMBER CORRECTION AND SOFT TISSUE PRESERVA-
TION FOR ELECTRONIC CLEANSING IN CTC IMAGES
By Mr.Krisorn Chunhaponpipat
Field of Study Computer Science and Information Technology
Thesis Advisor Associate Professor Rajalida Lipikorn, Ph.D.
Thesis Co-advisor Sirod Sirisup, Ph.D.

Accepted by the Faculty of Science, Chulalongkorn University in Partial Fulfillment
of the Requirements for the Doctoral Degree

..... Dean of the Faculty of Science
(Associate Professor Polkit Sangvanich, Ph.D.)

THESIS COMMITTEE

..... Chairman
(Associate Professor Nagul Cooharajanane, Ph.D.)

..... Thesis Advisor
(Associate Professor Rajalida Lipikorn, Ph.D.)

..... Thesis Co-advisor
(Sirod Sirisup, Ph.D.)

..... Examiner
(Assistant Professor Ratinan Boonklurb, Ph.D.)

..... Examiner
(Associate Professor Anchali Krisanachinda, Ph.D.)

..... External Examiner
(Associate Professor Montri Maleewong, Ph.D.)

ไกรสร ชุณหพงษ์พิพัฒน์ : การแก้ไขเลขซีทีแปลกปลอมที่เพิ่มขึ้นให้ถูกต้องด้วยอนุพันธ์
อันดับสองตามแนวผิวสัมผัสและการเก็บรักษาเนื้อเยื่ออ่อนสำหรับการล้างลำไส้ใหญ่ใน
ภาพรังสีส่วนตัดอาศัยคอมพิวเตอร์. (GRADIENT DIRECTIONAL SECOND
DERIVATIVE PEH CT NUMBER CORRECTION AND SOFT TISSUE
PRESERVATION FOR ELECTRONIC CLEANSING IN CTC IMAGES)
อ.ที่ปรึกษาวิทยานิพนธ์หลัก : รศ.ดร.รัชลิดา ลิปิกรณ์, อ.ที่ปรึกษาวิทยานิพนธ์ร่วม :
ดร.ศิโรจน์ ศิริทรัพย์ 99 หน้า.

วิทยานิพนธ์ฉบับนี้เสนอวิธีการล้างลำไส้ใหญ่ในภาพรังสีส่วนตัดอาศัยคอมพิวเตอร์ สอง
วิธี ซึ่งสามารถแก้ปัญหาเหล่านี้คือ ชั้นสิ่งแปลกปลอมที่รอยต่อของอากาศกับกากอาหาร เลข
ซีทีที่แปลกปลอม ความกำกวมระหว่างชั้นรอยต่อของอากาศกับอุจจาระกับชั้นเนื้อเยื่ออ่อน
บางระหว่างอากาศกับอุจจาระ และ สิ่งแปลกปลอมที่รอยต่อสามองค์ประกอบ วิธีแรกใช้การ
แก้ไขค่าซีทีสแกนที่เพิ่มขึ้นแฝงด้วยอนุพันธ์อันดับสองตามแนวผิวสัมผัส และแยกชั้นรอยต่อของ
อากาศกับอุจจาระกับชั้นเนื้อเยื่ออ่อนบางระหว่างอากาศกับอุจจาระออกจากกันโดยดัดแปลง
วิธีค่าความหนาแน่นเฉพาะส่วน ดังนั้นอุจจาระสามารถถูกลบโดยใช้วิธีตัดค่าอย่างง่าย วิธีที่สองรวม
อนุพันธ์อันดับสองตามแนวผิวสัมผัสเข้ากับแบบจำลองอัตราส่วนองค์ประกอบเพื่อเก็บรักษาจุด
ภาพของเนื้อเยื่ออ่อนที่มีค่าซีทีแปลกปลอมที่เพิ่มขึ้น และ กำจัดชั้นสิ่งแปลกปลอมที่ชั้นรอย
ต่อของอากาศกับอุจจาระและรอยต่อสามองค์ประกอบ การระบุสิ่งแปลกปลอมที่ชั้นรอยต่อ
ของอากาศกับอุจจาระถูกเสนอเพื่อเก็บชั้นเนื้อเยื่ออ่อนบางระหว่างอากาศกับอุจจาระไว้ ผล
จากการประเมินทางคลินิกแสดงถึงความเชื่อถือได้เมื่อเปรียบเทียบกับวิธีที่มีอยู่และซอฟต์แวร์
ทางการค้า

ภาควิชา	คณิตศาสตร์และ	ลายมือชื่อนิสิต
	วิทยาการคอมพิวเตอร์	ลายมือชื่อ อ.ที่ปรึกษาหลัก
สาขาวิชา	วิทยาการคอมพิวเตอร์	
	และเทคโนโลยีสารสนเทศ	
ปีการศึกษา	2559	ลายมือชื่อ อ.ที่ปรึกษาร่วม

5473101523: MAJOR COMPUTER SCIENCE AND INFORMATION TECHNOLOGY

KEYWORDS: COMPUTED TOMOGRAPHY COLONOGRAPHY / PSEUDO-ENHANCEMENT
EFFECT / ELECTRONIC CLEANSING / PARTIAL VOLUME EFFECT

KRISORN CHUNHAPONGPIPAT : GRADIENT DIRECTIONAL SECOND DERIVATIVE PEH CT NUMBER CORRECTION AND SOFT TISSUE PRESERVATION FOR ELECTRONIC CLEANSING IN CTC IMAGES. ADVISOR : ASSOC. PROF. Rajalida Lipikorn, Ph.D., COADVISOR : Sirod Sirisup, Ph.D., 99 pp.

This dissertation proposes two electronic cleansing (EC) methods in Computed Tomography Colonography. These methods can solve the problems in EC which are the artifact partial volume effect at an AT layer, pseudo-enhancement (PEH) effect, the ambiguity between AT and ATT layers, and the artifacts at T-junctions. The first proposed EC method removes fecal-tagging material (FTM) using a simple thresholding method after applying the gradient directional second derivative (GDSD) PEH correction method to solve the PEH effect and the modified local roughness to separate AT layers from ATT layers. The second proposed EC method integrates GDSD into material fraction model to preserve PEH soft-tissue voxels and remove FTM and artifacts at AT layers and T-junctions. AT layers can be distinguished from ATT layers using the AT layer identification to preserve ATT layers. The results from clinical evaluation by the radiologist show reliability and improvement of the proposed method when comparing with the existing method and commercial software.

Department : Mathematics and
Computer Science

Field of Study : Computer Science
and Information Technology

Academic Year : 2016

Student's Signature

Advisor's Signature

Co-advisor's Signature

Acknowledgements

In the completion of my dissertation, I am deeply indebted to my advisors who are Associate Professor Dr. Rajalida Lipikorn, Assistant Professor Dr. Ratinun Boonklurb, and Dr. Sirod Sirisup. They do not only advice me on my research but also broaden my academic vision and support me to come this far. I would like to express my special thanks to my thesis committee: Associate Professor Dr. Nagul Cooharajanane, Associate Professor Dr. Anchali Krisanachinda and Associate Professor Dr. Montri Maleewong for their invaluable suggestions and comments. Moreover, I feel thankful to all of my teachers who had taught me knowledge and skills. Also, I wish to express my thankfulness to my family and my friends for their encouragement throughout my study.

Contents

	Page
Abstract (Thai)	iv
Abstract (English)	v
Acknowledgements	vi
Contents	vii
List of Tables	x
List of Figures	xi
Chapter	
1 Introduction	1
1.1 Objectives	7
1.2 Scope of Work	7
1.3 Hypothesis	8
1.4 Expected Outcome	8
1.5 Thesis Overview	8
2 Pseudo-enhancement of CT number correction for fecal-tagging	
CTC image	10
2.1 Adaptive correction of the pseudo-enhancement of ct attenuation for fecal-tagging ct colonography	10
2.2 Fast pseudo-enhancement correction in ct colonography using linear shift-invariant filters	12
2.3 Scale-based scatter correction for computer-aided polyp detection in ct colonography	14
3 Electronic cleansing methods in CTC image	17
3.1 Classifying CT image data into material fractions by a scale and rota- tion invariant edge model	17
3.2 Fold-preserving electronic cleansing using a reconstruction model inte- grating material fractions and structural responses	21

Chapter	Page
3.3 Fast three-material modeling with triple arch projection for electronic cleansing in CTC	23
3.4 Structure-analysis method for electronic cleansing in cathartic and non-cathartic CT colonography	27
4 The proposed EC methods	32
4.1 The first proposed EC method	34
4.1.1 Lung and bone removal	34
4.1.2 Colonic lumen detection	36
4.1.3 The gradient directional second derivative PEH correction	36
4.1.4 Ambiguous layer detection	39
4.1.5 AT layer segmentation	39
4.1.6 The proposed EC method	40
4.1.7 Colonic lumen enhancement	42
4.2 The second proposed EC method	42
4.2.1 AT layer identification	42
4.2.2 Three material fractions approximation	44
4.2.3 Integration of gradient directional second derivative and three-material fraction model	47
5 Experimental results and conclusion	50
5.1 The first proposed EC method evaluation	50
5.1.1 CTC data set detail	50
5.1.2 Clinical evaluation	51
5.1.3 PEH correction Evaluation	52
5.1.4 Objective Evaluation	55
5.1.5 Visual Assessment	58
5.2 The second proposed EC method evaluation	61

Chapter	Page
5.2.1 CTC data set detail	61
5.2.2 Clinical evaluation	61
6 Discussion and Conclusion	68
6.1 Discussion	68
6.2 Conclusion	69
References	70
APPENDICES	75
Biography	84

List of Tables

Table	Page
1.1 Sensitivity and specificity of polyp detection in laxative-free CTC screening . . .	6
1.2 Sensitivity and specificity of polyp detection in optical colonoscopy (OC)	6
4.1 The observed standard CT number of each material in HU [2]	33
5.1 Grading scheme in cleansing quality evaluation	51
5.2 Five causes for low quality EC	51
5.3 Numbers of the remaining per the existing of submerged folds in four intervals. .	58
5.4 The numbers of actual polyps from CTC data of King Chulalongkorn Memorial Hospital.	58
5.5 Grading scheme in cleansing quality evaluation	61
5.6 Five causes for low quality EC	62
5.7 Volume of the remaining artifacts at T-junctions after applying EC_{prop}	63
5.8 Comparing the preference of the remaining artifacts at T-junctions after applying ECs between EC_{prop} and EC_{syngo}	63
5.9 Comparison between the results from EC_{prop} and EC_{prev} [11]	64
1 XOR result between ground truth and result of the first proposed EC method .	77
2 List of abbreviations	83

List of Figures

Figure	Page
1.1 A picture of colon and rectum from : http://www.webmd.com/digestive-disorders/picture-of-the-colon	2
1.2 Progression from polyp to cancer from : http://www.hopkinscoloncancercenter.org	2
1.3 Virtual colonoscopy from : http://www.thelancetnorway.com/journals/lanonc/article/PIIS1470-2045(13)70216-X/fulltext	4
1.4 CTC scanner from : http://qct.com/mindwaysct-receives-510k-clearance-for-no-dose-bone-densitometry-technology	4
3.1 Edge of material transition is used to form the triangle where vertices are represented by the pure material CT number of three materials which air, ST, and FTM.	24
3.2 The measurement data $\{I, \theta\sigma_w I_w\}$ is orthogonally projected onto three arches where projected points on arches are used to calculate the material fractions.	24
4.1 The first proposed EC process	34
4.2 Lung removal process (a) CTC image (b) the result from background removal (c) the result from lung removal	35
4.3 Colonic lumen detection result (a) CTC image (b) the area of colon in CTC image (c) the area of colon represented by white in black background	36
4.4 Submerged fold on the left and the GDSG characteristics of edges on the right (a) submerged fold which is shown in the visible CT number range from -1024 HU to 1024 HU (b) GDSG which can be used to identify submerged lesion and fold are shown in the visible range from -1.0 to 1.0	37
4.5 The regions of interest (ROI) of the ambiguous layers (a) The blue arrow points at AT layer and the red arrow points at ATT layer (b) The binary image represents the location of ambiguous layers (c) The result from ambiguous layer thinning (d) The result from using the local roughness [2] (e) The result from using the modified local roughness in (4.5)	41

Figure	Page
4.6 EC final result of the first proposed EC method (a) a ROI CTC image for illustrating hole filling operation (b) the floating artifact voxel and stair step edge (c) EC final result after applying hole filling operation the floating artifact voxel disappear and blurring the stair step effect	42
4.7 The second proposed EC process	43
4.8 Result of Ambiguous layer detection, AT layer identification and STT layer detection (a) CTC image with the ambiguous layers (b) the ambiguous layers in binary image (c) CTC image with AT layer (d) AT layer in binary image (e) CTC image with STT layer (f) STT layer in binary image	46
4.9 $\{I, \theta\sigma_\omega I_\omega\}$ is represented by star. $\{I', \theta\sigma_\omega I'_\omega\}$ is the red circle on $arch(I')$. The red circle is the intersection point of orthogonal line to tangent line of $arch(x)$. $(I', \theta\sigma_\omega I'_\omega)$ on $arch(I')$ is used to find material fraction.	48
4.10 a result of the second proposed EC method (a) the CTC image Blue arrows point at AT layers that are removed at the same time as FTM Red arrows point at ATT layers that are preserved from EC (b) the axial final result from our second proposed method	49
5.1 The first row contains region of interest (ROI). The second row contains volume of interest (VOI) of the first row. (a) ROI of a CTC image (b) ROI of EC of a CTC image (c) VOI of a CTC image (d) VOI of EC of a CTC image	52
5.2 The first row contains ROI. The second row contains VOI of the first row. (a) ROI of a CTC image (b) ROI of EC of a CTC image (c) VOI of a CTC image (d) VOI of EC of a CTC image	53
5.3 CT number profile of a submerged fold (a) ROI of a CTC image (b) ROI from ADC result (c) ROI from our first proposed EC (d) profile of CT numbers where y -axis represents CT number and x -axis represents location of pixel in ROI image	54

Figure	Page
5.4 CT number profile of a submerged fold (a) ROI of a CTC image (b) ROI from ADC result (c) ROI from our first proposed EC (d) profile of CT numbers where y -axis represents CT number and x -axis represents location of pixel in ROI image	55
5.5 CT number profile of pedunculate polyp. (a) ROI of a CTC image (b) ROI from ADC result (c) ROI from our first proposed EC (d) profile of CT numbers where y -axis represents CT number and x -axis represents sample pixels from (a), (b) and (c)	56
5.6 The comparison process between binary image of ground truth and the results of the first proposed EC method (a) A sample CTC image with ROIs in the small rectangle (b) A binary image of the ground truth with ROIs in the small rectangle (c) Labeled ROIs of the ground truth (d) Labeled ROIs of the result at the same position as the ground truth	57
5.7 The comparison of axial view between the result using only thresholding and the result from the first proposed EC method is used. The comparison of VOI between a result with and without applying the first proposed EC method is used. (a) The ambiguous case (b) The blue arrow points at PVE between air and FTM components which is an AT layer and the red arrow points at the thin ST between air and FTM components which is an ATT layer (c) The remaining layers after FTM removal using threshold, 200 HU (d) ROI of our first proposed EC result (e) VOI of original CTC image volume (f) VOI of our first proposed EC result from using paraview software	59
5.8 The first proposed EC method for IFTM case (a) The ambiguous case which contains both AT and ATT layers (b) FTM and AT layers were removed correctly and an ATT layer is preserved by our first proposed EC method (c) The IFTM case (d) The result after applying our first proposed EC to IFTM case	60

Figure	Page
5.9 Comparison of results of T-junction artifacts removal between the second proposed EC method and EC_{syn-go} (a) the axial CTC image of EC result from the second proposed EC method (b) the axial CTC image of EC result from EC_{syn-go} (c) the axial CTC image without applying any EC (d) the 3-D band view of (a) (e) the 3-D band view of (b) (f) the 3-D band view of (c)	64
5.10 Comparison of results of AT or PV effect layer removal between the second proposed EC method and EC_{syn-go} (a) the axial CTC image of EC result from the the second proposed EC method (b) the axial CTC image of EC result from EC_{syn-go} (c) the axial CTC image without applying any EC (d) the 3-D band view of (a) (e) the 3-D band view of (b) (f) the 3-D band view of (c)	65
5.11 Comparison of results of polyp preservation between the second proposed EC method and EC_{syn-go} (a) the axial CTC image of EC result from the second proposed EC method (b) the axial CTC image of EC result from EC_{syn-go} (c) the axial CTC image without applying any EC (d) the 3-D band view of (a) (e) the 3-D band view of (b) (f) the 3-D band view of (c) . . .	65
5.12 Comparison of results of ATT layers preservation between the second proposed EC method, EC_{prop} and the fast three-material model [11], EC_{prev} (a),(d),(g) and (j) are the axial CTC image of EC result from EC_{prop} (b), (e),(h) and (k) are the axial CTC image of EC result from EC_{prev} (c),(f), (i) and (l) are the axial CTC image without applying any EC	66
5.13 Comparison of result of ATT layer preservation in 3-D band view between the second proposed EC, EC_{prop} , and the fast three-material model [11], EC_{prev} (a) the axial CTC image of EC result from EC_{prop} (b) the axial CTC image of EC result from EC_{prev} [11] (c) the axial CTC image without applying any EC (d) the 3-D band view of (a) (e) the 3-D band view of (b) (f) the 3-D band view of (c)	67

Figure	Page
5.14 Comparison of result of fold preservation in 3-D band view between the second proposed EC, EC_{prop} and the fast three-material model [11], EC_{prev} (a) the axial CTC image of EC result from EC_{prop} (b) the axial CTC image of EC result from EC_{prev} [11] (c) the axial CTC image without applying any EC (d) the 3-D band view of (a) (e) the 3-D band view of (b) (f) the 3-D band view of (c)	67
1 (a) a CTC image (b) ground truth (c) boundary of the ground truth (d) boundary of the first proposed EC result	78
2 (a) Dilation of Fig. 1(c) with square element structure element size 2 (b) Dilation of Fig. 1(c) with square element structure element size 3 (c) Dilation of Fig. 1(c) with square element structure element size 4 (d) Dilation of Fig. 1(c) with square element structure element size 5	79

CHAPTER I

INTRODUCTION

In the US, Colorectal cancer [26] is the third most general cancer and the third cause of death in men and women. In 2014, there were approximately 136,830 people with colorectal cancer and 50,310 people died from this disease. These causes of cancers and deaths could be avoided by following the knowledge of cancer prevention and regular colorectal cancer screening and standard treatment for all patients. Ten years ago, in the U.S., there was no prevention and detection of colorectal cancer using colorectal cancer screening to reduce the number of diagnoses and death from colorectal cancer. Although, in 2010, people of age 50 or older were recommended to have colorectal cancer screening but only 59% of them followed the recommendation.

The effective colorectal cancer screening can help to avoid colorectal cancer due to the capability of polyp detection in the colon and rectum. However, not all of the polyps become cancer but polyp removal can prevent cancer from developing. Moreover, the colorectal cancer screening can possibly detect colorectal cancer at an early stage after it has developed which increases the chance of curing. This curing is more pleasant and it heals faster. To reduce the risk of developing and dying from colorectal cancer, it is suggested to follow the recommended screening guidelines and to have healthy lifestyle with normal body weight, regular routine exercise, healthy food, no alcohol and no smoking. Colorectal cancer surviving is given high priority by the American Cancer Society according to the efficiency of the screening technique based on existing knowledge that can prevent cancer, reduce suffering, and save lives.

Colorectal cancer is found in the colon or the rectum as shown in Fig. 1.1. Colorectal cancer depends on the location within the colon or rectum. For instance, tumors in the right colon are common among women and older patients while tumor in left colon are more general among men and younger patients. Colorectal cancer takes time to develop which is longer than 10 to 20 years. Normally, a noncancerous growth developed inside

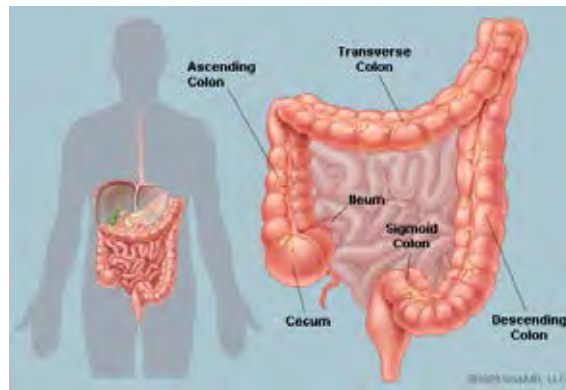


Figure 1.1: A picture of colon and rectum from : <http://www.webmd.com/digestive-disorders/picture-of-the-colon>

colon or rectum is called a polyp. The most general kind of polyp is called an adenomatous polyp or adenoma. Adenomas originates from the glandular cells, which generates mucus for colorectum lubricant. Although most of adenomas possibly become colorectal cancer, less than 10% are developed as invasive cancer. The adenomas sizes increase are possible to develop into cancer. Adenocarcinomas are cancer that develop from glandular cells and approximately 96% of colorectal cancer are adenocarcinomas as shown in Fig. 1.2.

Since cancer is embeded in the inner lining of colon, it develops inside the colonic

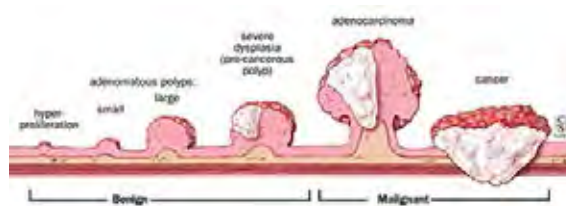


Figure 1.2: Progression from polyp to cancer from : <http://www.hopkinscoloncancercenter.org>

wall or rectum. Then, it can spread into the circulatory and lymphatic system. Cancerous cells can be transported to nearby lymph nodes, liver, lung, pelvis, and other organs via blood vessels. The spread of cancer can determine the stage of cancer and be used to decide the choices of treatment. There are several ways to describe the stage of cancer but the two most common staging systems are TNM and SEER systems. First is the TNM (Tumor, Node, Metastasis) system which is normally used in clinical settings. Sec-

ond is the Surveillance, Epidemiology, and End Result (SEER) summary staging system, which is used for descriptive and statistical analysis of tumor registry data. The SEER summary staging system is as follows:

In situ refers to cancers that have not yet embedded inside the colon or rectum wall; this lesion are not included in the cancerous statistic report.

Local refers to cancers that have developed into the lining of colon or rectum, but have not spread to nearby tissues.

Regional refers to cancers that have spread to nearby tissues or nearby lymph nodes.

Distant refers to Cancers that have invaded to other organs of the body such as liver and lung.

However, there is no symptom for the early stage of colorectal cancer. According to the slow growth from precancerous polyp to invasive cancer, the chances of detecting and preventing colorectal cancer are available. Thus, the screening is important. The screening can prevent cancer by detecting and removing the precancerous growths before it develops into cancer. As a consequences, the screening decreases colorectal cancer mortality by reducing the incidence of disease and increasing the rate of survival. There are several colorectal cancer screenings for both genders of age 50 or older such as:

Flexible sigmoidoscopy: The sigmoidoscope is about 2 feet long (60 cm) with a slender, flexible, hollow, lighted tube which is inserted through the rectum into colon for visibility inside rectum and the lower one-third of the colon or sigmoid colon. This screening requires enemas for bowel preparation without sedation. If there is the present of polyp or tumor, there is the need for colonoscopy to further examine the entire colon.

Colonoscopy: This is similar to sigmoidoscopy but the flexible endoscope is much longer, more complex instrument, enabling examiner to view the entire colon and to remove polyps. This technique requires the laxative agents to perfectly clean the colon. Sedation is generally used to minimize the inconvenienc feeling during the examination. If the polyp is detected, it is possible to be removed during the examination. This is the most sensitive method for adenomatous polyp or colorectal cancer detection. If the examination is negative, a patient can come back again in the next 10 years for colorectal cancer screening. However, the limitations of the colonoscopy are the missing rates of 20% for all

adenomas and 10% for large (5mm or larger) or advanced adenomas. Another limitation is the bowel tearing and bleeding, especially when a polyp is removed.

Computed tomography colonography (CTC): Also known as virtual colonoscopy,

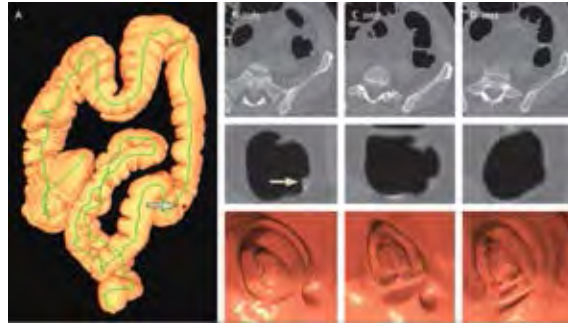


Figure 1.3: Virtual colonoscopy from : [http://www.thelancetnorway.com/journals/lanonc/article/PIIS1470-2045\(13\)70216-X/fulltext](http://www.thelancetnorway.com/journals/lanonc/article/PIIS1470-2045(13)70216-X/fulltext)



Figure 1.4: CTC scanner from : <http://qct.com/mindwaysct-receives-510k-clearance-for-no-dose-bone-densitometry-technology>

this technique, which has been used since 1990s, is capable of visualizing cross-sectional, 2-or 3-dimensional view inside the entire colon and rectum via collaboration of a special x-ray machine and a computer as shown in Fig. 1.3. However, bowel cleansing is needed but there is no sedation for CTC. In order to expand the size of colonic bowel in CTC, a small flexible tube is inserted into the rectum and inflate the colon using air or carbon dioxide before a patient goes through a CTC scanner. The CTC scanner as shown Fig.

1.4 generates multiple images of the interior of colon. The advantage of CTC over other screening examinations is that a patient needs no recovery time and it takes only 10 or 15 minutes to finish. A polyp with significant size of 5mm or other abnormal results are submitted to colonoscopy. To detect invasive cancer or polyp with size larger than 1 cm, the existing studies have reported that the performance of CTC is similar to optical colonoscopy.

A CTC image that is generated from a CTC scanner consists of three main components: air, soft-tissue, and feces or stool. Each voxel in CTC data is represented by a number, called CT attenuation or CT number. CT number of a voxel is calculated by comparing the transmitted radiation from the X-ray to the observed component with the transmitted radiation from the X-ray to water [27]. However, CT number of soft tissue and stool are in the same range. To be able to distinguish soft tissue from feces in CTC images, the feces are tagged using ingested contrast agents, called fecal-tagging material [12]. CT numbers of fecal-tagging materials are lightened to be as high as bones which are brighter than the surrounding soft-tissue components. Fecal-tagging materials can be subtracted digitally from CTC images, this is called electronic cleansing (EC) [12, 13] or digital bowel cleansing (DBC) [32, 33]. CTC cases can be publicly retrieved from Walter Reed Army Medical Center for the quality of EC evaluation which were prepared by Pickhardt *et al.* [19]. Pickhardt *et al.*'s prepared patients by giving them underwent a standard 24-hour colonic preparation with oral administration of 90 ml of sodium phosphate and 10 mg of bisacodyl. Oral contrast agents consist of 500 ml of barium for solid-stool tagging and 120 ml of diatrizoate meglumine and diatrizoate sodium for fecal tagging. The multidetector CT scanning was used to acquire CTC images in both supine and prone positions with 1.25-2.5 mm collimation, a table speed of 15mm/s, a reconstruction interval of 1 mm, a tube current of 100 mA, and a voltage of 120 kVp. In general, there are approximately 500 slices of CTC images with 512×512 for each case. The CT numbers are from -1000 to 3000 HU. Note that a 3-D view inside the entire colon is reconstructed from CT numbers of air components which can be obtained in full capacity from rectum to the entire colon in CTC images using EC.

EC allows the radiologists to visualize polyps under fecal-tagging material pools

Table 1.1: Sensitivity and specificity of polyp detection in laxative-free CTC screening

measure	size \geq 6mm	size \geq 8mm
sensitivity	0.59	0.7
specificity	0.88	0.86

Table 1.2: Sensitivity and specificity of polyp detection in optical colonoscopy (OC)

measure	size \geq 6mm	size \geq 8mm
sensitivity	0.76	0.88
specificity	0.94	0.91

in CTC images. There is the recent performance of EC reported by Pickhardt *et al.* [20]. For polyp with the diameter size from 6 mm to 9mm, the sensitivity and specificity of polyp detection are 86%. For polyp with the diameter size larger than 10 mm or 1 cm, the sensitivity and specificity of polyp detection are 93% and 97%, respectively. As the requirement of CTC, the laxative or cathartic for colonic bowel cleansing is used as same as optical colonoscopy (OC) screening [4]. This preparation makes the patients uncomfortable which gives negative feeling for the follow-up colorectal cancer screening [23, 29, 30, 6]. The initiative study of non-cathartic or laxative-free with contrast agent on patients yields the patient-friendly examination [3]. Later, there is the collaboration among groups that study the performance of CTC with laxative-free comparing to OC screening [34]. For adenomas of size 10 mm or larger, per-patient sensitivity of CTC is 0.91 and specificity is 0.85 while sensitivity of OC is 0.95 and specificity is 0.89. For adenomas of size 8mm or larger, sensitivity of CTC is 0.7. For adenomas of size 8mm or larger, sensitivity and specificity of OC are 0.88 and 0.91, respectively. For adenomas of size 6mm or larger, sensitivity of CTC is 0.59. For adenomas of size 6mm or larger, sensitivity and specificity of OC are 0.76 and 0.94, respectively. Specificity of OC is better than that of CTC which are 0.86 for 8 mm or larger and 0.88 for 6 mm or larger ($P = 0.02$) as shown in Tables. 1.1 and 1.2. Although, virtual colonoscopy with cathartic is the major obstruction for patients to come back and follow the screening schedule but the recent performance of EC with cathartics is very promising. There is another study [11] that reports the EC performance using 15 patients with 27 polyps of size 6 mm, i.e., 54 polyps in 30 scans. Among them, 37 out of 54 polyps can be found easily because they are surrounded by air. For the rest of them, they are partially or completely covered by fecal-tagging material. For the other three existing methods [25, 10, 11], they have the same 100% sensitivity of polyp detection.

Colorectal cancer is the third cause of death which occur mostly to people of age 50 or older. There are just 59% of them who go for colorectal screening. The screening can prevent colorectal cancer by removing adenomas polyp in the early stage. There are several screening methods but the most sensitive one for polyp detection is optical colonoscopy. However, a patient may not want to have this screening because of the irritation and harmfulness during insertion of optical endoscope through the entire colon. The virtual colonoscopy is the alternative choice for colorectal cancer screening according to high rate of sensitivity and specificity of polyp detection. To diagnose the colorectal cancer from virtual colonoscopy, the full colonic volume needs to be obtained from air voxels inside colon in CTC data. Electronic cleansing is proposed to reveal polyps under fecal-tagging material (FTM) by subtracting FTM from CTC images.

1.1 Objectives

The Objectives of this dissertation is to propose a novel method that can:

1. remove the artifacts at air-tagging (AT) layers in CTC
2. preserve the pseudo-enhancement (PEH) soft tissue (ST) voxels after performing EC.
3. preserve the thin ST layer between air and FTM or air-tissue-tagging (ATT) layer.
4. remove the artifacts at T-junctions where air, ST, and FTM meet simultaneously.
5. consume time complexity less than $O(n^3)$.
6. to compare the proposed method with the existing methods and commercial software for evaluation.

1.2 Scope of Work

We study EC in CTC image with laxative and oral contrast agent in bowel preparation.

1.3 Hypothesis

The hypothesis for the first proposed EC method are as follows:

- The proposed PEH correction reduce CT numbers as high as 500 HU into ST range.
- The proposed EC method preserve ATT layers.
- Null hypothesis:
 - H_{0A}^1 :The goodness of cleansing has the global mean relative error of our proposed methods is higher than or equal to 0.1%.
- Alternative hypothesis:
 - H_{1A}^1 :The goodness of cleansing has the global mean relative error of our proposed methods is less than 0.1%.

The hypothesis for the second proposed EC method is that the improvement of preference of radiologist to the proposed EC method is higher than 20% from a recent existing method.

1.4 Expected Outcome

A novel EC method in CTC with laxative and oral contrast agent in bowel preparation is proposed to remove the artifacts at AT layers and T-junctions and preserve all ST voxels in vicinity of FTMs which is considered to more powerful than the existing methods by abdominal radiologist's opinion.

1.5 Thesis Overview

The dissertation is organized as follows. In Chapter II, the pseudo-enhancement effect which leads to the problem of over cleansing in EC is explained and the pseudo-enhancement reduction which enhances the voxels in CTC images is explored. In Chapter

III, the existing electronic cleansing methods are reviewed, then the advantages and disadvantages of those methods are pointed out. In Chapter IV, the proposed EC method that can solve PEH problem, AT and ATT layers, and artifacts at three-material junctions is explained. For the PEH problem, the gradient directional second derivative is used to detect ST in vicinity of FTM. The proposed function is used to change CT numbers of PEH voxels around fecal-tagging materials. To improve the efficiency, the gradient directional second derivative is integrated into material fraction model of material transition between ST and fecal-tagging material. The Air-tagging (AT) and Air-Tissue-Tagging (ATT) layer whose voxels in these layers are similar to each other is described. In order to distinguish AT layers from ATT layers, the modification of local roughness function is proposed. However, the computational consumption is high when the the modification of local roughness function is used. Thus, the AT layer detection is proposed to reduce time complexity during the process of distinguishing AT layers from ATT layers. In Chapter V, the experimental results and comparison results between the proposed EC method and the existing methods are described.

CHAPTER II

PSEUDO-ENHANCEMENT OF CT NUMBER CORRECTION FOR FECAL-TAGGING CTC IMAGE

For fecal-tagging CTC, the residual bowel materials are opacified using oral contrast or tagging agents to increase ability to distinguish feces from ST components and to, especially, increase the visibility for colorectal lesion detection in a CTC image. However, the high radiodensity or CT number of FTM from oral contrast tends to artificially elevate CT numbers of the vicinity of FTM (in Hounsfield unit (HU) scale). FTM tends to introduce PEH that is the incorrectly incremental observed ST CT numbers near FTM [31, 21]. To correct CT numbers of PEH voxels, several methods [15, 28, 1, 14] were proposed to reduce or correct CT numbers of STs around FTM region to be in its belonging ST class.

2.1 Adaptive correction of the pseudo-enhancement of ct attenuation for fecal-tagging ct colonography

The adaptive density-correction (ADC) method [15] was introduced to correct CT numbers of the vicinity of FTM. This algorithm is an iterative model that estimates an energy distribution which is generated from high-density regions in CT data. There are two main steps of the algorithm. In the first step, the total PEH energies of FTM are approximated. In the second step, the distribution of the estimated PEH energy from FTM is approximated as an expanding wave front with decreasing energy.

Let v_p represent the observed CT number of a voxel p and let \hat{v}_p represent the actual CT number of p without the effect of PEH. Thus, the observed CT number of p

can be approximated as

$$v_p = \hat{v}_p + v_p^{\text{PEH}}, \quad (2.1)$$

where v_p^{PEH} is the PEH at p . Finally, the actual CT number can be approximated by subtracting the v_p^{PEH} from the observed CT number which can be calculated from

$$\hat{v}_p = v_p - v_p^{\text{PEH}} \approx v_p - \sum_{i=0}^n r^i(p), \quad (2.2)$$

where $v_p^{\text{PEH}} \approx \sum_{i=0}^n r^i(p)$. To approximate v_p^{PEH} , the total PEH energy received at p from the neighboring voxels, q , of p is approximated by

$$r^0(p) = \sum_q r_q^0(p), \quad (2.3)$$

where the initial PEH energy, $r_q^0(p)$, received at a voxel p from a voxel $q \neq p$ is approximated by

$$r_q^0(p) = \frac{e_q}{\sqrt{2\pi}\sigma_1(v_q)} \exp\left(-\frac{1}{2} \left(\frac{\mathcal{D}(p,q)}{\sigma_1(v_q)}\right)^2\right), \quad (2.4)$$

where $\sigma_1(v_q)$ is the Gaussian spread of the energy parameter as a function of the observed CT number of q and $\mathcal{D}(p,q)$ is the Euclidean distance between voxels q and p such that the location of q is in the coverage of p , where $1 + \lceil 2\sigma_1(v_q) \rceil$ is the distance between q and p voxels and $\tau_q \in \mathbf{R}$ is a thresholding parameter, $\tau_q = 100$ HU. The use of lower threshold τ_q cannot differentiate CT numbers of FTM from CT numbers of ST components [16]. The PEH energy, e_q , at q is calculated by

$$e_q = \begin{cases} v_q - \tau_q, & \text{if } v_q > \tau_q, \\ 0, & \text{otherwise,} \end{cases} \quad (2.5)$$

Next, the total residual energy received at p at iteration i can be approximated by

$$r^i(p) = \sum_q \frac{r^{i-1}(q)}{\sqrt{2\pi}\sigma_2(r^{i-1}(q))} \exp\left(-\frac{1}{2} \left(\frac{\mathcal{D}(p,q)}{\sigma_2(r^{i-1}(q))}\right)^2\right), \quad (2.6)$$

where $\sigma_2(r^{i-1}(q))$ is the Gaussian spread parameter of the redistributed residual energy at q . The function parameters $\sigma_1(v)$ and $\sigma_2(r)$ in (2.3) and (2.6) are modeled as

$$\sigma_1(v) = av + b, \sigma_2(r) = cr + d, \quad (2.7)$$

where a, b, c and d are parameters that were optimized to reduce the high CT number within the ST regions to the range of 50–100 HU from phantoms. The iteration of (2.6) is terminated when the additive effect of the remaining redistributable energy becomes less than 10 HU. To be more precise, Tsagaan *et al.* [28] found that the function parameters in previous ADC method [15] should be a nonlinear function rather than just a linear function which could be formed as

$$\sigma_1(v) = a \exp\left(\frac{v_q - b}{c}\right) + d \text{ and } \sigma_2(r) = c \exp\left(\frac{r}{f}\right) + g. \quad (2.8)$$

2.2 Fast pseudo-enhancement correction in ct colonography using linear shift-invariant filters

To accelerate the speed of PEH correction, Boyes *et al.* [1] proposed the fast PEH correction using a linear shift-invariant filter. This method performs on CTC image plane using the two-dimensional shift-variant Gaussian filtering. The shift variance relates linearly to CT number in Gaussian model. The convolution between a linear shift-variant filter and a tagging image [17] as follows:

$$y[n_1, n_2] = \sum_{k_1} \sum_{k_2} t[k_1, k_2] h_{k_1, k_2}[n_1 - k_1, n_2 - k_2], \quad (2.9)$$

where $t[n_1, n_2]$ is a CTC image with FTM and $h_{k_1, k_2}[n_1 - k_1, n_2 - k_2]$ is a shift-variant isotropic Gaussian filter,

$$h_{k_1, k_2}[k_1, k_2] = \frac{1}{2\pi\sigma^2} \exp\left[-\frac{((k_1 - m_1)^2 + (k_2 - m_2)^2)}{2\sigma^2}\right], \quad (2.10)$$

where $[m_1, m_2]$ is the center point of a filter and $\sigma[m_1, m_2]$ is a linearly spatially-varying standard deviation depended on $t[m_1, m_2]$. A tagging image $t[n_1, n_2]$ is obtained from

$$t[n_1, n_2] = \begin{cases} x[n_1, n_2] - T, & x[n_1, n_2] > T, \\ 0, & \text{otherwise,} \end{cases} \quad (2.11)$$

where $x[n_1, n_2]$ is the original CTC image and T is a threshold which equals to 100 HU. The PEH corrected image can be obtained by subtracting the result in (2.9) from the original CTC image. However, the process of filtering a CTC image of size $N \times N$ with a filter of size $M \times M$ directly takes $O(N^2M^2)$ operations.

To speed up the process, the fast convolution method is applied using fast Fourier transform (FFT). Unfortunately, the fast convolution cannot be used with the spatially varying standard deviation. Thus, CT numbers are divided into L bands where each band will convolute with certian standard deviation. This idea will change the approximation of the linear shift-variant filter into the fast linear shift-invariant (LSI) filter where $t_i[n_1, n_2]$ in each band can be divided as follows:

$$t_i[n_1, n_2] = \begin{cases} t[n_1, n_2], & B_i < t[n_1, n_2] \leq B_{i+1} \\ 0, & \text{otherwise,} \end{cases} \quad (2.12)$$

where $B_i = t_{min} + i(t_{max} - t_{min})/L$ are CT number thresholds that determine the band for $i \in [0, L]$. Therefore, each i^{th} band have the correspondent Gaussian filter as

$$h_i[n_1, n_2] = \frac{1}{2\pi\sigma_i^2} \exp^{-\frac{((n_1-m_1)^2+(n_2-m_2)^2)}{2\sigma_i^2}}, \quad (2.13)$$

where $\sigma_i(x) = -0.0004x + 0.59$ and x is CT number. Finally, the convolution in (2.9) is performed using the shift-invariant filtering with the banded images, i.e; $y[n_1, n_2] \approx \sum_i t_i[n_1, n_2] * h_i[n_1, n_2]$, where t_i stands for the thresholded image for i^{th} band obtained from (2.12). To summarize the time-complexity from L bands, each 2D shift invariant filter approximation directly takes $O(LM^2N\log_2N)$. Furthermore, the time complexity

can be reduced to $O(LMN\log_2 N)$ by performing the separable dimension in FFT domain of the shift-invariant Gaussian.

The algorithm for the shift-invariant PEH correction is performed as follow:

1. Initialize PEH image $P = 0$ where P is used to store result of convolution.
2. $L =$ Numbers of bands.
3. Compute bands $B_i = t_{min} + i(t_{max} - t_{min})/L$.
4. **for** $i = 0$ **to** $L - 1$ **do**.
 - (a) lower = bands(i).
 - (b) upper = bands($i + 1$).
 - (c) Compute linear kernal h_i given σ_i .
 - (d) Compute banded image b_i .
 - (e) Compute thresholded banded image t_i from b_i .
 - (f) Convolve t_i and h_i and add to P .
5. **end for**.
6. Subtract P from original CTC image.

2.3 Scale-based scatter correction for computer-aided polyp detection in ct colonography

Liu *et al.* [14] developed a scale-based correction method that minimizes scatter effects in CTC data by subtracting the estimated scatter components from observed CT number. This method [14] consists of three steps:

1. compute the object scale for a given CTC images
2. estimate scatter components

3. subtract the estimated scatter components from the CT number

First, the scale of each voxel c , $K(c)$, is defined as the radius of the largest hyperball. The center of this hyperball is at a voxel c where all voxels within the ball satisfy a predefined CT number homogeneity criterion. For any voxel c in a CTC image, a digital ball with radius r centered at c , contains a set of voxels $B_r(c) = \{d \mid \|d - c\| \leq r\}$ where $\|d - c\|$ is the distance between c and d . The homogeneity fraction, $FO_r(c)$, is used to indicate the fraction of the ball boundary occupied by a region that is homogeneous with c by

$$FO_r(c) = \frac{\sum_{d \in B_r(c)} W(f(c) - f(d))}{|B_r(c) - B_{r-1}(c)|}, \quad (2.14)$$

where $|B_r(c) - B_{r-1}(c)|$ is the number of voxels in volume of $|B_r(c) - B_{r-1}(c)|$, $f(c)$ is CT number of voxel c and $W(x)$ is a homogeneity function defined as

$$W(x) = \exp^{-x^2/2}. \quad (2.15)$$

At the beginning, the scale, $K(c)$, of a voxel c is set to 1. The ball with radius r is iteratively increased and is estimated the fraction of the object $FO_r(c)$ containing c that is contained in the ball. For the first time that this fraction is lower than a predefined constant, $K(c)$ is set to be r due to this radius contains an object region different from what c belongs. The value of $K(c)$ is small at the location close to the boundary and high at the location far away from the boundary. $K(c)$ is used for the adaptive scatter function to estimate the scatter components.

The distribution of scatter components, I_s , is approximated by convolving a CTC image I_0 with an adaptive symmetric scatter function $SF(c)$:

$$I_s = I_0 \otimes SF(c), \quad (2.16)$$

where

$$SF(c) = \left(\frac{1}{\sqrt{\pi\sigma}} \right)^2 \exp^{-((x-u)^2 + (y-v)^2)/\sigma^2}. \quad (2.17)$$

The parameters of the scatter function, u, v and σ are adaptively set as the transform scale values derived from:

$$u = v = 0.5(S_c - K(c)) \text{ and} \quad (2.18)$$

$$\sigma = S_c - K(c) \quad (2.19)$$

where S_c is a parameter of maximum scale value which is set in the scale computation algorithm. This scatter function $SF(c)$ is adaptive and spatially variant according to depends on the density and distribution of contrast agent. The transform scale is used to explain the region of scatter effects of ST influenced by the neighboring contrast agents. Finally, CT number are corrected by subtracting of the estimated scatter component I_s from CT numbers at each voxel c :

$$\hat{I}_t = I_0 - I_s. \quad (2.20)$$

The PEH correction methods can correct CT number of ST around FTM. The corrected CT numbers of STs are preserved from disappearing after applying EC methods, especially, polyps and folds that partially or completely submerged in FTM. After applying PEH correction method, EC is performed in order to remove FTM from a CTC image. For the next chapter, some of EC methods will be explored.

CHAPTER III

ELECTRONIC CLEANSING METHODS IN CTC IMAGE

FTM in CTC image may cover polyps when performing the 3D fly-through navigation inside colon. Thus, there should be a method that can remove FTM in a CTC image to reveal a suspicious ST lesion which is partially or completely submerged in FTM. Electronic Colon Cleansing (ECC) or Electronic Cleansing (EC) was developed to remove FTM in CTC images.

3.1 Classifying CT image data into material fractions by a scale and rotation invariant edge model

Several EC methods have been proposed. For instance, Serlie *et al.* [24] proposed the EC method that considers the CT number of a voxel in CTC data that is a mixing of the CT numbers of two materials. Thus, there would be a fraction of low CT number material and a fraction of high CT number material for a voxel. In order to approximate the material fractions of a voxel, Serlie *et al.* [24] classified CT image data into material fractions by the scale and rotation invariant edge model. This method does not depend on the scale of anisotropic Gaussian filter or edge orientation where the anisotropic Gaussian filter depends on the sampling pitch in each axes. The relationship between CT number and the first derivative along gradient direction value of a voxel can be plotted as scatter points that look like an arch where one base of the arch is the mean of the low CT number material and the another base is the mean of the higher CT number material between two materials. The generalized arch function describes the scale-normalized gradient $\sigma_w I_w$ as a function of the intensity, here is known as CT number, I and the expected values L and H

$$\text{arch}(I; L, H) = (H - L) \text{arch}\left(\frac{I - L}{H - L}\right), \quad (3.1)$$

where I is CT number, I_w is the first derivative along gradient direction and σ_w is the scale of edge. The function $\text{arch}(x)$ is used to describe the scale-invariant gradient magnitude $\sigma_w I_w$ as a function of I as follows:

$$\begin{aligned}\text{arch}(x) &\triangleq \sigma g(G^{-1}(x; \sigma); \sigma) \\ &= \frac{1}{\sqrt{2\pi}} \exp(-\{\text{erf}^{-1}(2x - 1)\}^2),\end{aligned}\tag{3.2}$$

where $\text{erf}^{-1}(\cdot)$ is the inverse of the error function. The effective scale of edge σ_w in the gradient direction was modeled by [25] as a function of the angle α between the gradient vector and the positive z -axis.

$$\sigma_w(\alpha) = \sqrt{(\sin(\alpha)\sigma_{\perp z})^2 + (\cos(\alpha)\sigma_z)^2},\tag{3.3}$$

where σ is the scale of the out-of-plane underlying Gaussian erf and $\sigma_{\perp z}$ is the scale of the in-plane underlying Gaussian erf which is the Gaussian edge-spread function as follows:

$$g(x; \sigma) = \frac{1}{\sigma\sqrt{2\pi}} \exp\left(\frac{-x^2}{2\sigma^2}\right).\tag{3.4}$$

After CT number I and the scale-normalized gradient $\sigma_w I_w$ are obtained as above, the noise in $(I, \theta\sigma_w I_w)$ can be isotropic. The noise in $(I, \theta\sigma_w I_w)$ is made isotropic by

$$\theta = \frac{1}{\sigma_w} \left(\frac{\sigma_I}{\sigma_{I_w}} \right) = \frac{1}{\sigma_w} \left(\frac{\sqrt{2}\sigma_{op,w}^{3/2}\sigma_{op,\perp w}}{\sqrt{\sigma_{op,z}\sigma_{op,\perp z}}} \right),\tag{3.5}$$

where $\sigma_{op,z}$ is the axial scale and $\sigma_{op,\perp z}$ is the lateral scale of the Gaussian operator with respect to the z -direction and $\sigma_{op,w}$ is the effective scale of the Gaussian operator in the gradient direction w that is defined as a function of the angle α_Δ between z and w

$$\sigma_{op,w}(\alpha_\Delta) = \sqrt{(\sin(\alpha_\Delta)\sigma_{op,\perp z})^2 + (\cos(\alpha_\Delta)\sigma_{op,z})^2},\tag{3.6}$$

and $\sigma_{op,\perp w}$ is the effective scale of the operator in the direction of vector ν that is perpendicular to gradient direction w that is defined as a function of the angle γ_Δ between

z and ν

$$\sigma_{op,\perp w}(\gamma_\Delta) = \sqrt{(\sin(\gamma_\Delta)\sigma_{op,\perp z})^2 + (\cos(\gamma_\Delta)\sigma_{op,z})^2}. \quad (3.7)$$

For optimal σ_z and $\sigma_{\perp z}$, the calibration was performed by Serlie *et al.* [25] using the fitting the erf function in a representative image to each edge voxel for estimating σ_w where the erf function is expressed as:

$$G(w; L, H, \sigma_w) = L + (H - L) \left(\frac{1}{2} + \frac{1}{2} \operatorname{erf} \left(\frac{w}{\sigma_w \sqrt{2}} \right) \right). \quad (3.8)$$

Consequently, σ_z and $\sigma_{\perp z}$ are estimated by fitting (3.3). This yields an in-plane scale of ~ 0.40 mm and an out-of-plane scale of ~ 0.82 mm. Thus, σ_w is possible to be approximated for any edge having orientation α by mean of (3.3) using calibrated values of σ_z and $\sigma_{\perp z}$.

To approximate the material fractions of a voxel from a material transition, the bases of that material transition must be approximated. The bases of a material transition between two components can be approximated by minimizing the summed squared residuals between the arch and the measurement where the measurement is $(I, \theta\sigma_w I_w)$. To minimize the summed squared residuals between the arch and the measurements, the measurements are used to find the orthogonal projection of a measurement pair onto an arch $(I', \theta\sigma_w I'_w)$. The orthogonal projection of a measurement pair onto an arch $(I', \theta\sigma_w I'_w)$ uses the closed-form inverse arch function arch^{-1} as (3.9) and its derivative as (3.10) to approximate numerically where arch^{-1} can be expressed as:

$$\operatorname{arch}^{-1}(x) = \frac{1}{2} - \frac{1}{2} \operatorname{erf} \left(\sqrt{-\ln(x\sqrt{2\pi})} \right) \quad (3.9)$$

and the derivative of inverse arch function can be expressed as:

$$\frac{d}{dx} \operatorname{arch}^{-1}(x) = (-\ln(2\pi) - 2\ln x)^{-\frac{1}{2}}. \quad (3.10)$$

Let $y = q(x, C)$ be the line that is orthogonal to $\text{arch}^{-1}(x)$ with slope k and y intercept m ($0 \leq m \leq \frac{1}{2}$), which crosses $\text{arch}^{-1}(x)$ at point $C = (x_c, y_c)$ and (y_c, x_c) is the orthogonal projection of a measurement pair onto an arch of $(I, \theta\sigma_w I_w)$. All measurements $(\theta\sigma_w I_w, I)$ on this line are projected onto point C of $\text{arch}^{-1}(x)$

$$k = \left(\frac{d}{dx} \text{arch}^{-1}(x) \right)^{-1} \Big|_{x=x_c} \quad (3.11)$$

$$m = -k * x_c + \text{arch}^{-1}(x_c)$$

$$y = q(x, C) = kx + m \quad (3.12)$$

$$= \frac{x_c - x}{\frac{d}{dx} \text{arch}^{-1}(x) \Big|_{x=x_c}} + \text{arch}^{-1}(x_c).$$

For a particular measurement ($x = \theta\sigma_w I_w$, $y = I$), x_c can be numerically obtained by solving (3.12) for individual $(\theta\sigma_w I_w, I)$ and y_c is calculated from substitution of x_c into (3.9), $y_c = \text{arch}^{-1}(x_c)$. The obtained (x_c, y_c) or $(I', \theta\sigma_w I'_w)$ is called $\text{proj}_{\text{arch}}(L, H, \theta)$. Let L' and H' be the optimal values that minimize the summed squared residuals between the arch and the measurements as follows:

$$\{L', H'\} = \arg \min_{\{L, H\}} \sum_n \|A_n - \text{proj}_{\text{arch}(L, H, \theta)}\|^2, \quad (3.13)$$

where A is a set of $N + 1$ measurement pairs along the gradient direction in neighborhood of an edge.

Finally, $(I', \theta\sigma_w I'_w)$ the orthogonal projection of the sample onto the arch with the optimal L' and H' is used to find β_L and β_H material fractions in a voxel as follows:

$$\beta_L = \frac{I' - L'}{H' - L'}, \quad \beta_H = \frac{H' - I'}{H' - L'} \quad \text{and} \quad \beta_L + \beta_H = 1. \quad (3.14)$$

After material fractions of a voxel are obtained, EC can be performed at the voxel that have FTM fraction higher than other component fractions. However, the PEH effect

to vicinity of FTM voxels, Ravesteijn *et al.* [22] notice that the candidate objects (polyps) of high intensity (CT number), here is CT number, are removed by the previous EC method [24]. To solve this problem, Lee *et al.* [10] proposed the fold-preserving electronic cleansing using a reconstruction model integrating material fractions [24] and structural responses.

3.2 Fold-preserving electronic cleansing using a reconstruction model integrating material fractions and structural responses

To preserve the submerged folds under FTM, the rut-enhancement function [2] is used by Lee *et al.* [10] to enhance the submerged folds based on local structural features rather than CT number. Let the eigenvalues of Hessian matrix at a voxel be λ_1 , λ_2 and λ_3 ($|\lambda_1| \leq |\lambda_2| \leq |\lambda_3|$) and their corresponding eigenvectors be e_1 , e_2 and e_3 , respectively. The eigenvalue signature is used to explain the local morphologic structure of an object using the combination of the eigenvalues. In general, the submerged fold has CT number lower than FTM with concave ridge (i.e., rut-like shape). The concave structure with the transition from submerged fold to FTM has the positive λ_3 . For $\lambda_3 > 0$, λ_1 is approximated to be zero because of no change in curvature along the ridge axis e_1 of the fold. For eigenvectors e_2 and e_3 , they represent the height axis and the thickness axis of the fold and perpendicular to e_1 , respectively. Since the height is significantly larger than the thickness, the proportion between the eigenvalues of λ_2 and λ_3 is inversely where λ_2 and λ_3 respond for e_2 and e_3 , respectively. Therefore, the characteristic of the structure of submerged folds can be expressed using the eigenvalue signature as $\lambda_3 > 0$, $\lambda_1 \approx 0$ and $\lambda_2 \ll \lambda_3$.

For the rut-enhancement function [2], it is based on the eigenvalue signature that corresponds to structure of submerged fold as follows:

$$F_{rut} = F_A \cdot F_B, \quad (3.15)$$

where F_A is used to differentiate between elongate shape and sphere which is expressed

as

$$F_A = \exp\left(-\frac{R_a^2}{2\alpha^2}\right) \text{ and } R_a = \frac{|\lambda_1|}{\sqrt{|\lambda_2\lambda_3|}} \quad (3.16)$$

and F_B is used to characterize the rut-like structure in cross section of the ridge axis of the rut.

$$F_B = \exp\left(-\frac{(R_b - \gamma)^2}{2\beta^2}\right) \text{ and } R_b = \frac{|\lambda_2|}{|\lambda_3|} \quad (3.17)$$

and the parameters α, β and γ are experimentally set as 0.7, 0.4 and 0.3, respectively.

From the material fraction model [24], CT number $I_{material-fraction}$ of a voxel in the vicinity of edge between FTM and ST can be modeled by linear combination of pure material CT number of these two materials using the corresponding material fraction:

$$I_{material-fraction} = t_{ST} \cdot I_{ST} + t_{FTM} \cdot I_{FTM}, \quad (3.18)$$

where t_{ST} and I_{ST} are the corresponding material fractions of ST component and pure material CT number of ST component obtained from base L' of material transition between ST and FTM, respectively. t_{FTM} and I_{FTM} are the corresponding material fractions of FTM and pure material CT number of FTM obtained from base H' of material transition between ST and FTM, respectively. In order to solve problem of material fraction that was discovered by Ravesteijn *et al.* [22], the rut-enhancement function was embedded into the material fraction model (3.18) by Lee *et al.* [10] as follow:

$$\begin{aligned} I_{fold-preserving} &= \left(1 - (1 - F_{rut})^k\right) \cdot I + (1 - F_{rut})^k \cdot I_{material-fraction} \\ &= t_{ST} \cdot I_{ST} + t_{FTM} \cdot \left[\left(1 - (1 - F_{rut})^k\right) \cdot I_{FTM} + (1 - F_{rut})^k \cdot I_{air}\right], \end{aligned} \quad (3.19)$$

where I_{air} is the pure material CT number of air component obtained from base L' of material transition between air and FTM and a parameter k is set as 2. At this stage, so far, the submerged folds are preserved from the erroneous EC due to PEH effect.

3.3 Fast three-material modeling with triple arch projection for electronic cleansing in CTC

Although the submerged folds under tagged pools in a CTC image have been preserved using EC method from Lee *et al.* [10] but there are still some remaining artifacts at junction of three materials in the EC results where three materials are air, ST, and FTM, respectively. The junction that air, ST and FTM meet simultaneously, is called T-junction. In order to remove the artifacts at T-junction, Lee *et al.* [11] proposed the fast three-material modeling with triple arch projection for electronic cleansing in CTC. The triangle edges can be used to represent three transitions between two materials. First material transition is between air and ST. Second material transition is between air and FTM. The last material transition is between ST and FTM. The vertices of the triangle represent CT number of three pure materials which are air, ST and FTM. The arches from three transitions of two materials coincide with the edges of the triangle in a barycentric coordinate as shown in Fig. 3.1. Therefore, for each voxel, the measurement $\{I, \theta\sigma_w I_w\}$ is perpendicularly projected onto the closest points on three arch curves where each arch is the transition of two materials as shown in Fig. 3.2. Three arch-projected points (**APs**) in three arch curves are used to approximated three pairs of two-material fractions. Since three materials represent the barycentric coordinate, the location of three pairs of **APs** are on an edge of the triangle as follows:

$$\begin{aligned}
 \mathbf{AP}_{air-ST} &= t_{air/(air-ST)} \cdot P_{air} + t_{ST/(air-ST)} \cdot P_{ST}, \\
 \mathbf{AP}_{air-FTM} &= t_{air/(air-FTM)} \cdot P_{air} + t_{FTM/(air-FTM)} \cdot P_{FTM} \text{ and} \\
 \mathbf{AP}_{ST-FTM} &= t_{ST/(ST-FTM)} \cdot P_{ST} + t_{FTM/(ST-FTM)} \cdot P_{FTM},
 \end{aligned} \tag{3.20}$$

where P_{air} , P_{ST} , and P_{FTM} are three vertices of triangle corresponding to single material of air, ST and FTM, respectively. Additionally, $t_{A/(A-B)}$ is the material fraction of A

between two materials A and B which can be derived from:

$$\begin{aligned}
 t_{air/(air-ST)} + t_{ST/(air-ST)} &= t_{air/(air-FTM)} + t_{FTM/(air-FTM)} \\
 &= t_{ST/(ST-FTM)} + t_{FTM/(ST-FTM)} \quad (3.21) \\
 &= 1.
 \end{aligned}$$

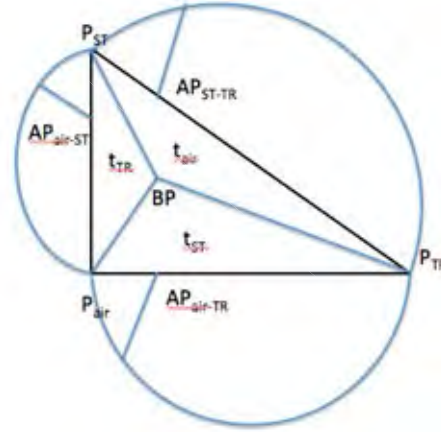


Figure 3.1: Edge of material transition is used to form the triangle where vertices are represented by the pure material CT number of three materials which air, ST, and FTM.

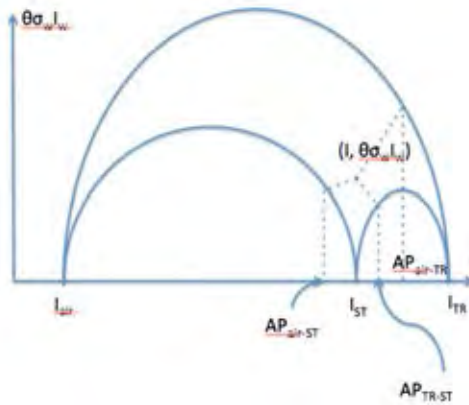


Figure 3.2: The measurement data $\{I, \theta_w I_w\}$ is orthogonally projected onto three arches where projected points on arches are used to calculate the material fractions.

To generate a single barycentric point (**BP**) in the interior of the triangle, the

barycentric interpolation of the three **AP**s is used as follows:

$$\mathbf{BP} = \alpha_{air-ST} \cdot \mathbf{AP}_{air-ST} + \alpha_{air-FTM} \cdot \mathbf{AP}_{air-FTM} + \alpha_{ST-FTM} \cdot \mathbf{AP}_{ST-FTM}, \quad (3.22)$$

where

$$\alpha_{air-ST} + \alpha_{air-FTM} + \alpha_{ST-FTM} = 1, \alpha_{air-ST} = \alpha_{air-FTM} = \alpha_{ST-FTM} = \frac{1}{3}. \quad (3.23)$$

Notice that Lee *et al.* [11] assumed that an arbitrary voxel in the T-junction has an unbiased distribution of the predominance of each material. For **BP** with uniform weights, The center of the triangle is formed by three **AP**s as follows:

$$\begin{aligned} \mathbf{BP} &= \frac{1}{3} (\mathbf{AP}_{air-ST} + \mathbf{AP}_{air-FTM} + \mathbf{AP}_{ST-FTM}) \\ &= \frac{t_{air/(air-ST)} + t_{air/(air-FTM)}}{3} \cdot P_{air} \\ &\quad + \frac{t_{ST/(air-ST)} + t_{ST/(ST-FTM)}}{3} \cdot P_{ST} \\ &\quad + \frac{t_{FTM/(air-FTM)} + t_{FTM/(ST-FTM)}}{3} \cdot P_{FTM}, \end{aligned} \quad (3.24)$$

where

$$\begin{aligned} &t_{air/(air-ST)} + t_{air/(air-FTM)} + t_{ST/(air-ST)} + t_{ST/(ST-FTM)} \\ &\quad + t_{FTM/(air-FTM)} + t_{FTM/(ST-FTM)} = 3. \end{aligned} \quad (3.25)$$

The areas of three sub-triangles in the triangle determine the position of **BP**. The areas of three sub-triangles are proportional to the fraction of each material. Finally, the material fractions of air, ST, and FTM can be approximated as follows:

$$\begin{aligned} t_{air} &= \frac{t_{air/(air-ST)} + t_{air/(air-FTM)}}{3} \\ &= \frac{t_{ST/(air-ST)} + t_{ST/(ST-FTM)}}{3} \\ &= \frac{t_{FTM/(air-FTM)} + t_{FTM/(ST-FTM)}}{3} = 1 - t_{air} - t_{ST}. \end{aligned} \quad (3.26)$$

After the material fractions of air, ST and FTM are obtained, the linear combination

of the pure material CT number of air, ST and FTM with the corresponding material fractions can be used to calculate the CT number $I_{original}$ as follows:

$$I_{original} = t_{air} \cdot I_{air} + t_{ST} \cdot I_{ST} + t_{FTM} \cdot I_{FTM}. \quad (3.27)$$

To perform EC using three material fractions, the linear combination of the pure material CT numbers of air and ST with material fractions t_{air} , t_{ST} and t_{FTM} models the CT number, $I_{fractions}$, as follow:

$$I_{fractions} = t_{air} \cdot I_{air} + t_{ST} \cdot I_{ST} + t_{FTM} \cdot I_{air}. \quad (3.28)$$

To preserve the submerged fold, the rut-enhancement function is embedded into three-material model as weight factor in the same manner that was used in Lee *et al.* [10]. Finally, CT number, $I_{fold-preserving}$, of the integration of rut-enhancement function and three material fractions is modeled as follows:

$$\begin{aligned} I_{fold-preserving} &= (1 - (1 - F_{rut})^k) \cdot I_{original} + (1 - F_{rut})^k \cdot I_{fractions} \\ &= t_{air} \cdot I_{air} + t_{ST} \cdot I_{ST} \\ &\quad + t_{FTM} \cdot \{(1 - (1 - F_{rut})^k) \cdot I_{FTM} + (1 - F_{rut})^k \cdot I_{air}\} \end{aligned} \quad (3.29)$$

The advantage of EC of Lee *et al.* [11] is the fold preservation, the artifact at T-junction removal and low complexity. However, there are still the some issues that need to be concerned. Cai *et al.* [2] pointed out that there is similarity between ATT layer and AT layer where ATT layer is the thin ST layer between air and FTM while AT layer is the artifact thin layer between air and FTM. These AT and ATT layers are not handled by Lee *et al.* [10, 11]. Furthermore, Lee *et al.* [11] did not pay attention to the polyp preservation where polyp has cup-like structure.

3.4 Structure-analysis method for electronic cleansing in cathartic and non-cathartic CT colonography

Because there are still the drawbacks in EC of Lee *et al.* [11], EC method of Cai *et al.* [2] proposed an number EC that can take care of the submerged folds and polyps under FTM and the similarity between AT and ATT layers. The structural response functions have been proposed to preserve the implicit shape of cup-like and rut-like structures. The local roughness response function has also been proposed to preserve voxels in ATT layer. Let $I(\mathbf{x})$ be CT number of a point $\mathbf{x} = (x, y, z) \in \mathbb{R}^3$ where \mathbf{x} is in the 3D Euclidean space. The Hessian matrix with size 3×3 is used to find eigenvalues of a voxel where Hessian matrix H is expressed as follows:

$$H = \begin{Bmatrix} f_{xx} & f_{xy} & f_{xz} \\ f_{yx} & f_{yy} & f_{yz} \\ f_{zx} & f_{zy} & f_{zz} \end{Bmatrix}, \quad (3.30)$$

where f_a and f_{ab} are the first and second partial derivatives of $I(\mathbf{x})$ which can be approximated by the convolution of the first and second partial derivatives of Gaussian function and I :

$$\begin{aligned} f_a &= \frac{\partial I(\mathbf{x})}{\partial a} \cong \left(\frac{\partial}{\partial a} G_{0;\sigma}(\mathbf{x}) \right) * I(\mathbf{x}), \\ f_{ab} &= \frac{\partial^2 I(\mathbf{x})}{\partial a \partial b} \cong \left(\frac{\partial^2}{\partial a \partial b} G_{0;\sigma}(\mathbf{x}) \right) * I(\mathbf{x}), \end{aligned} \quad (3.31)$$

where $G_{0;\sigma}(\mathbf{x})$ is an isotropic Gaussian function with a mean value of 0 and a standard deviation of σ or smoothing kernel. To emphasize on scale-parameter σ , for smoothing kernel, Cai *et al.* [2] explained that image structures of spatial size smaller than σ are smoothed away in the scale-space level at scale σ^2 . Thus, they set σ to one voxel unit, μ , to smooth away structures smaller than one voxel where $\mu = 1$. The multiscale Hessian matrix was calculated over two scales which are μ and 2μ . For the eigenvalue signatures of submerged folds and polyps under FTM, the polyps are presented as cup-like (concave cap) structures and the folds are presented as rut-like (concave ridge) structures.

The eigenvalue signature for submerged folds was in literatures of Lee *et al.* [10] and [11]. The submerged polyps, λ_1 , λ_2 and λ_3 are characterized by eigenvalue signatures of $\lambda_3 > 0$, $\lambda_1 \approx \lambda_2$ and $\lambda_2 \propto \lambda_3$. The cup-like structural enhancement function F_{cup} is used for preserving polyp under FTM which is expressed as follows:

$$F_{cup} = F_C(\lambda_1, \lambda_2) \cdot F_C(\lambda_2, \lambda_3), \quad (3.32)$$

where

$$F_C(\lambda_i, \lambda_j) = 1.0 - \exp\left(-\frac{R_c^2}{2\eta^2}\right) \text{ and } R_c = \frac{|\lambda_i|}{|\lambda_j|}, \quad (3.33)$$

where η controls the range of the enhancement function F_c which it could be set vary but it was chosen to be set as $\eta = 0.2$. Since there are two structural enhancement functions to detect whether a voxel is a cup-like structure or rut-like structure, the response from these two functions are compared. However, these two structural enhancement functions are also calculated under the multiscale Hessian matrix. Thus, for a voxel, there are two rut-like structural responses and two cup-like structural responses for $\sigma = \mu$ and $\sigma = 2\mu$. The maximum response of structural enhancement function across σ is called the Hessian response field \mathcal{H} which is expressed as follows:

$$\mathcal{H} = \max_{\sigma=\mu}^{2\mu} \{F_{rut}(\mathbf{x}; \sigma), F_{cup}(\mathbf{x}; \sigma)\}. \quad (3.34)$$

The profiles of CT number and the gradient magnitude of voxels in AT and ATT layers have shown the similarity of patterns [2]. Thus, it is difficult to identify whether a voxel is in an AT or an ATT layer, by using only gradient magnitude. According to the local nonlinear volume averaging created partial volume (PV) effect layer between air and FTM, CT numbers of AT layer are more irregular than those of ATT layer. The irregularity of an AT layer is from the observation of CT number of voxels in both an AT layer and an ATT layer. The iso-valued voxels in an AT layer are often disconnected while those of thin ST structures as ATT layer are connected. This indicates that CT numbers of an AT boundary are more irregular than those of the this ST structures sandwiched within an ATT layer. Thus, Cai *et al.* [2] proposed the local roughness to measure this

irregularity.

The local roughness at point \mathbf{x} is defined as the cumulative of the difference between local volume curvedness of the consecutive scales σ as follows:

$$R(\mathbf{x}) = \sum_{i=1}^6 (B_i \cdot \Delta CV_i(\mathbf{x})^2), \quad (3.35)$$

where $\Delta CV_i(\mathbf{x}) = CV_{\sigma_i}(\mathbf{x}) - CV_{\sigma_{i-1}}(\mathbf{x})$ is the difference between local volume curvedness of the consecutive scales σ_i and σ_{i-1} and $B_i = 1$ for every i . The volumetric curvedness at point \mathbf{x} is approximated by

$$CV_{\sigma}(\mathbf{x}) = \sqrt{\frac{1}{2} (\kappa_1^{\sigma}(\mathbf{x})^2 + \kappa_2^{\sigma}(\mathbf{x})^2)}, \quad (3.36)$$

where $\kappa_1^{\sigma}(\mathbf{x})$ and $\kappa_2^{\sigma}(\mathbf{x})$ are the two principal curvatures at scale σ . The principal curvature can be approximated as

$$\kappa_1, \kappa_2 = K_M \pm \sqrt{K_M^2 - K_G} \quad (3.37)$$

where K_M and K_G are the mean curvature and Gaussian curvature [7], respectively. The Gaussian curvature can be approximated by

$$K_G = -\frac{\det \begin{vmatrix} H & \nabla F^T \\ \nabla F & 0 \end{vmatrix}}{|\nabla F|^4}, \quad (3.38)$$

where $\nabla F = \left(\frac{\partial f}{\partial x}, \frac{\partial f}{\partial y}, \frac{\partial f}{\partial z} \right)$. The mean curvature can be approximated by

$$K_M = \frac{\nabla F \times H \times \nabla F^T - |\nabla F|^2 \text{Trace}(H)}{2|\nabla F|^3}, \quad (3.39)$$

where $\text{Trace}(H)$ is the diagonal members of H . To characterize the voxels in an AT layer, the curvedness values are high at small scales and, in the contrast, they rapidly and monotonically decrease in the same manner as the curvedness values of the voxels in an ATT layer. The local roughness is used to reflect the relative change in curvedness.

Thus, it can effectively differentiate the AT layer from thin fold sandwiched within the ATT layer. However, the local roughness value varies across CTC images. The arctan function is used to compare the local roughness values in a normalized range. Therefore, the local roughness response field, \mathcal{R} , is defined as

$$\mathcal{R} = 1.0 - \frac{\tan^{-1}R}{0.5\pi}. \quad (3.40)$$

In EC method of Cai *et al.* [2], called the structure analysis (SA) cleansing method, the level set model from Ho *et al.* [8] is used with the structural response from eigenvalue signatures and the local roughness response. The SA cleansing method consists of five steps:

1. initial segmentation of the colon
2. compute the Hessian response field \mathcal{H}
3. compute the local roughness response \mathcal{R}
4. segment FTM using level set method
5. replace FTM obtained from previous step with air
6. reconstruct the colonic wall submerged in FTM

For the fourth step, the initializing of the level set front using FTM region obtained from the first step that is the region in colonic lumen with CT numbers higher than 200 HU. The level set front is iteratively evolved through the partial differential equation (PDE) as follows:

$$\frac{\partial \phi}{\partial t} = \{\mathcal{F}(g(\mathbf{x})) - \mathcal{F}(\mathcal{H}(\mathbf{x})) - \mathcal{F}(\mathcal{R}(\mathbf{x}))\}|\nabla \phi| + C_{curvature} \nabla \cdot \left(\frac{\nabla \phi}{|\nabla \phi|} \right) |\nabla \phi|, \quad (3.41)$$

where $g(\mathbf{x}) = |\nabla F(\mathbf{x})|$ and \mathcal{F} is a speed function defined as

$$\mathcal{F}(x) = \text{sign}(t(x)) \cdot |t(x)|^2, \quad (3.42)$$

and

$$t(x) = \begin{cases} -1, & \text{if } x < T - \Delta, \\ 1, & \text{if } x > T + \Delta, \\ \frac{x-T}{\Delta}, & \text{otherwise,} \end{cases} \quad (3.43)$$

where T is a threshold value obtained from using Otsu's thresholding method [18] and Δ is set to half of the difference between the threshold value and the peak value of the histogram of the enhanced objects. In the last step, called reconstruction of the transition layer, FTM that are segmented in the fourth step are replaced with air. The artificial transition boundary between the colonic walls and the subtracted FTM are reconstructed by the mucosa reconstruction method [33].

For the conclusion, there are still many EC methods that have been proposed. The EC methods of Cai *et al.* [2] and Lee *et al.* [11] are the recent EC methods that are used with patients given oral contrast and laxative. EC method of Lee *et al.* [11] takes care of the submerged folds under FTM and the artifact at T-junction without awareness of the similarity between AT and ATT layers while Cai *et al.* [2] have never mentioned about the artifact at T-junction removal.

CHAPTER IV

THE PROPOSED EC METHODS

From the previous chapters, there are three main problems for EC method. The first problem is the PEH effect problem. The second problem is the similarity between AT layer and ATT problem. The last problem is the artifacts at three-material junctions. These problems will be solved by the proposed EC.

For the first problem, the gradient directional second derivative (GDSD) is used to detect the locations of ST in the vicinity of FTM. After the locations of ST around FTM are detected, their CT numbers will be changed if they are higher than ST CT number range due to PEH effect. For the proposed PEH correction method, CT numbers of these ST voxels will be changed using simple linear transformation. The drawback of this proposed PEH correction method is the CT numbers of PEH voxels have to be known. The CT numbers of PEH voxels can approximately be from 100 to 600 HU. However, this interval is not consistent for every CTC data. The proposed PEH correction method can be improved by changing the CT numbers using the GDSD with linear combination of material fraction model. For the improved PEH correction method, the GDSD is embedded into a linear combination of material fraction model between ST and FTM.

For the second problem, CT numbers and gradient magnitudes of AT layers and ATT layers are similar to each other. The artifacts between air and FTM is generated from non-linear volume average which is called partial volume (PV) effect. The AT layer is PV effect layer which is needed to be removed. In contrast, the ATT layer is a thin ST layer between air and FTM which is needed to be preserved. For the existing methods, the local roughness was proposed to distinguish the voxels in AT layer from ATT layer. The local roughness is used as a forcing term in the level set method. However, the level set method segmentation highly takes computational time per time step of iteration. To reduce time

complexity, the layer labeling is used instead of the level set method. Thus, the modified local roughness method is proposed where it is compatible with the layer labeling. The modified local roughness expands the range of multiscale curvedness cumulative in AT layers and ATT layers to be easier to distinguish. The Otsu's thresholding method [18] is used to find the threshold to distinguish AT layers from ATT layers. For the voxels with modified local roughness higher than the threshold, they are removed. Although the computational time can be reduced by layer labeling with modified local roughness but the time complexity in the modified local roughness is not different from the local roughness. To reduce the time complexity in the modified local roughness, the AT layer detection is proposed by considering three directions of connectivity from layers to FTM in leaping distance where the CT scanner table must lie at bottom of CTC image.

For the last problem, the artifacts at three-material junctions are solved using three material fraction in linear combination. Three-material junctions (T-junction) are the location where air, ST, and FTM meet simultaneously. However, the material fraction model needs CT numbers and the first derivatives in gradient direction of voxels at edge between two materials. There are three types of edge. First is the edge between air and FTM which is AT layer. Second is the edge between air and ST. The last one is the edge between ST and FTM which is the layer obtained by subtraction AT layer from boundary of FTM. Since three materials fraction are obtained, the CT numbers at T-junction are changed using the linear combination of three-material fractions.

Table 4.1: The observed standard CT number of each material in HU [2]

Component	minimum	maximum
lumen air	-1000 HU	-800 HU
ST	-100 HU	100 HU
FTM	200 HU	1400 HU
AT Layer	-800 HU	600 HU

There are two proposed EC methods. The first one consists of the proposed PEH correction method and layer labeling with modified local roughness function as shown in Fig. ???. The second one consists of the AT layer detection and the integration of GDSD and material fraction model as shown in Fig. 4.7. For the next, the first proposed EC

method will be described and followed by the second proposed EC method.

4.1 The first proposed EC method

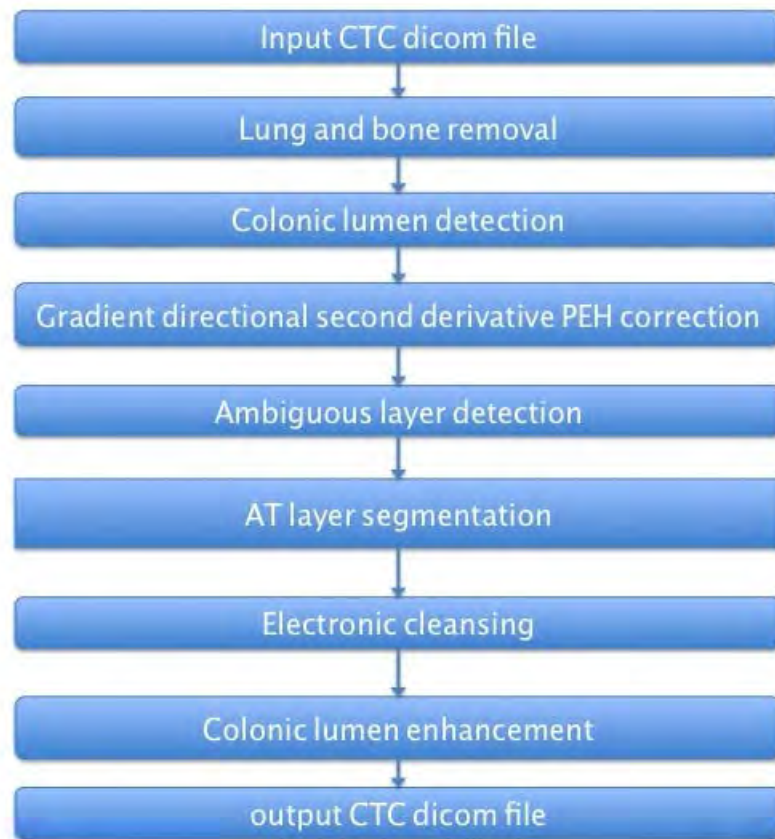


Figure 4.1: The first proposed EC process

4.1.1 Lung and bone removal

At the beginning, lungs and bones are removed in order to facilitate the rest of steps. Inside body, there are air and FTM inside colonic bowel while there also is air inside lungs. Furthermore, the CT numbers of FTM are similar to those of bone. Thus, in order to locate the colonic bowel precisely, the CT numbers of lungs and bones must be changed to ST CT number. Initially, air components are divided into two parts. The first one is inside body while another one is outside as shown in Fig. 4.2(a). The location of air component outside is detected using region growing of binary image. The initial seed points are placed at the boundaries of CTC image. To perform region growing, the seeds grow to the voxel with CT number lower than -100 HU. This is the minimum value

of ST CT number range as shown in Table. 4.1 where the result is shown in Fig. 4.2(b). Since obtained the location of air component outside body, the CT numbers of air outside body are changed to -100 HU. The air component inside body can only be processed. The lungs inside body can be located by considering the number of air voxels with CT numbers lower than -100 HU. There are two sides of CTC data which are the beginning and the end of CTC data. Ten slides from the beginning and ten slides from the end of a CTC data are used to consider the the number of air voxels. Due to the fact that lungs are located in the side with greater number of air voxels, the region growing of binary image is used to obtain all air voxels in lungs. The initial seeds are placed in the ten slides of the side with greater number of air voxels. The seeds grow to the voxels with CT number lower than -100 HU to obtain the location of lungs. After obtaining the location of lungs, the CT numbers of voxels inside lungs are changed to -100 HU as shown in Fig. 4.2(c). So far, air voxels are only inside colonic bowel. For bone component, there are bone components around lungs which are ribs. The locations of ribs around lungs are used as seeds for region growing of binary image to detect all bones in CTC data. Thus, the voxels with CT number higher than 200 HU around lungs are used as seeds where 200 HU is the minimum value of FTM and bone. The seeds grow to the voxels with CT number higher than 200 HU to obtain all voxels of bone component. After obtained bone voxels, CT number of bone voxels are changed into -100 HU.

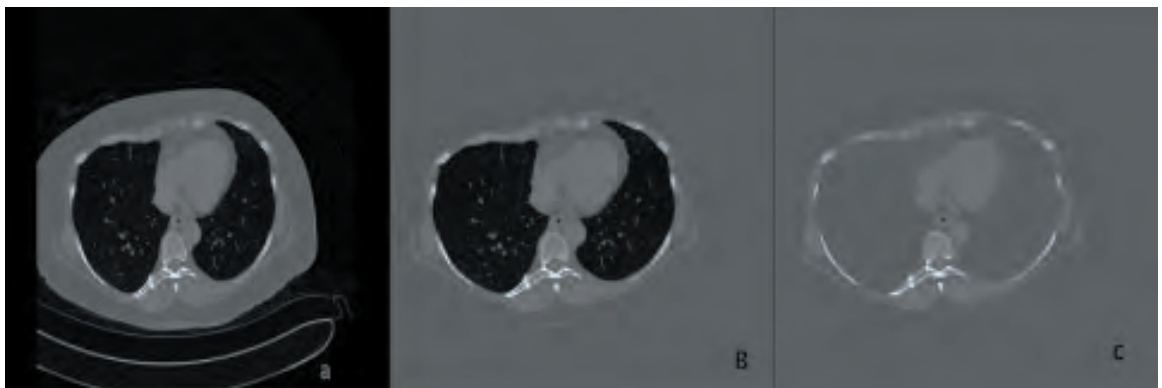


Figure 4.2: Lung removal process (a) CTC image (b) the result from background removal (c) the result from lung removal

4.1.2 Colonic lumen detection

Now, the colonic bowel can be obtained without interference from voxels of lungs and bones. The colonic bowel can be obtained by merging the FTM and air inside colonic bowel together. The binary image is used to represent the locations of volume of interest (VOI). The locations of FTM voxels can be detected which their CT number are higher than 200 HU. The morphological dilation with ball radius size 3 structural element is applied on the binary image of FTM where. radius size 3 is approximately the thickness of PV effect. The locations of air voxels can be detected which their CT number are lower than -600 HU. Finally, the colonic bowel is obtained by merging the binary image of FTM and air together as shown in Fig. 4.3.

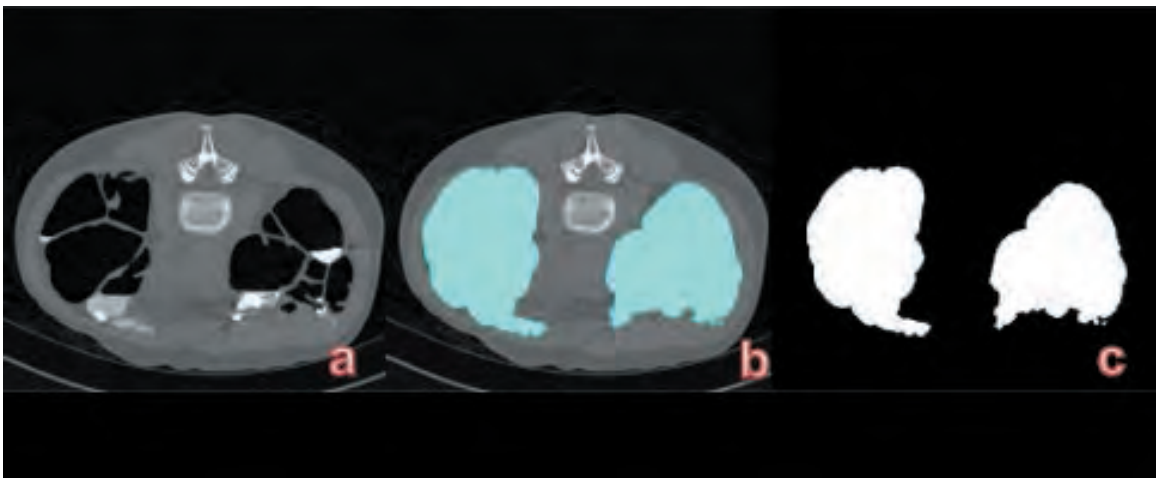


Figure 4.3: Colonic lumen detection result (a) CTC image (b) the area of colon in CTC image (c) the area of colon represented by white in black background

4.1.3 The gradient directional second derivative PEH correction

As explained before, the PEH correction or reduction method is used to change the CT number of ST around FTM. For the existing PEH correction methods [15, 28, 1, 14], they were proposed to reduce the CT numbers of voxels which are higher than 200 HU. This means not only the CT numbers of ST around FTM are reduced but the CT numbers of FTM are also reduced. There will be two problems from these approaches. First, after applied the PEH correction methods, the CT number of FTM could be lower than the

minimum CT number of FTM when the CT number of FTM is near the minimum CT number of FTM. Second, the CT number of ST would not be reduced to be in the CT numbers range of ST, $[-100, 100]$, when the CT number of PEH ST is higher than 500 HU. To solve this drawback, the GDSD is used in order to detect the PEH ST voxels around FTM and the proposed linear transformation is used to transform the CT number of the PEH ST voxels.

Before approximating the GDSD, the Gaussian image convolution will be performed. The Gaussian image convolution yields the Gaussian image f using Gaussian function G_σ and CTC data \bar{I} as an input. Let \bar{I} represents CTC data where $\bar{I}(\mathbf{x})$ is CT number at point $\mathbf{x} = [x \ y \ z]$ of three-dimensional Cartesian coordinate. The Gaussian image f can be obtained as follows:

$$f = \mathcal{F}^{-1}\{\mathcal{F}\{G_\sigma\} \cdot \mathcal{F}\{\bar{I}\}\}, \quad (4.1)$$

where $\mathcal{F}\{\cdot\}$ is the Fourier transform and $\mathcal{F}^{-1}\{\cdot\}$ is the inverse Fourier transform. $O(n \log n)$ is the complexities of Fourier transform and inverse Fourier transform [5] while the dot product between two Fourier transforms takes $O(n)$. The implementation detail can be found in Max *et al.* [9]. To preserved PEH ST voxels from EC removal, they will be reduced their CT number. However, folds and polyps can also completely or partially

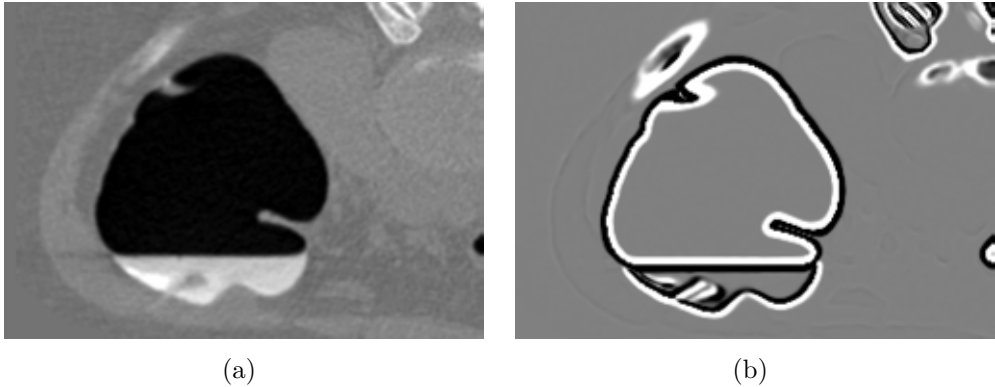


Figure 4.4: Submerged fold on the left and the GDSD characteristics of edges on the right (a) submerged fold which is shown in the visible CT number range from -1024 HU to 1024 HU (b) GDSD which can be used to identify submerged lesion and fold are shown in the visible range from -1.0 to 1.0

submerge under FTM which are one of ST component that need to be preserved. In order to detect the ST voxels around FTM, the GDSD is used. The Gaussian image f is used as input to calculate the GDSD as follows:

$$f_{\mathbf{nn}} = \frac{1}{|\nabla f| + C} (f_x f_x f_{xx} + f_y f_y f_{yy} + f_z f_z f_{zz} + 2f_x f_y f_{xy} + 2f_x f_z f_{xz} + 2f_y f_z f_{yz}), \quad (4.2)$$

where $|\nabla f| = \sqrt{f_x^2 + f_y^2 + f_z^2}$, f_a and f_{ab} are first and second partial second derivatives of Gaussian image f and C is positive constant. This study chooses $C = 1$ which does not change the physical meaning of (4.2).

For the characteristic of GDSD $f_{\mathbf{nn}}$, its magnitude will be high at edge between two components and it will be lower for voxels far away from edges. The high positive value represents rate of change at the edge from low CT number component to high CT number component. The high negative value represents rate of change at the edge from high CT number component to low CT number component. For vicinity of edge, there are two sides where the CT numbers of one side are lower than those of another one. For the lower sides, the GDSD are poistive as white line at vicinity of edge as shown in Fig. 4.4(b), while the black line at vicinity of edge are low negative. Thus, the positive GDSD are used to detect ST around FTM which can be used with CT number linear transformation of PEH voxels.

The linear transformation will be proposed to reduce the CT number of PEH ST voxels as follows:

$$\tilde{I}(\mathbf{x}) = \begin{cases} P(\bar{I}(\mathbf{x})), & L_{PEH} \leq \bar{I}(\mathbf{x}) \leq H_{PEH} \text{ and } f_{\mathbf{nn}} \leq t_G, \\ \bar{I}(\mathbf{x}), & \text{Otherwise,} \end{cases} \quad (4.3)$$

where the linear transformation P is

$$P(\nu) = L_{ST} + \left(\frac{\nu - L_{PEH}}{H_{PEH} - L_{PEH}} \right) (H_{ST} - L_{ST}), \quad (4.4)$$

which L_{ST} and H_{ST} are -100 and 100 HU, respectively. L_{PEH} and H_{PEH} are 100 and

600 HU where 100 HU is the minimum CT number that has PEH effect [15] while PEH ST voxels can be as high as 600 HU [2]. t_G is the threshold to locate vicinity of edge from $|f_{nn}|$ obtained by using Otsu's method [18]. After applying (4.3), the CT number of the PEH ST voxels will be reduced into standard ST range. Next, the AT and ATT layers will be detected as shown in Fig. 4.5(a) where the blue arrow points at AT layer and the red arrow points at ATT layer. They are called ambiguous layers since they are similar to each other [2].

4.1.4 Ambiguous layer detection

The boundary of air inside colonic bowel are composed of the edge between air and FTM and the edge between air and ST. To obtain ambiguous layers, the boundary of air inside colonic bowel is subtracted by the edge between air and ST. Thus, the remaining layers are the edge between air and FTM. To obtain the edge between air and ST, the 26 neighbor voxels are used. For the boundary voxels of air, if there are any voxels in the neighbor voxels have the CT number higher than 200 HU, that boundary voxels of air are removed. Thus, the remaining of boundary voxels of air are the edge between air and ST. The ambiguous layers can be obtained by subtraction the edge between air and ST from boundary voxels of air as shown in Fig. 4.5(b).

4.1.5 AT layer segmentation

Since obtained the ambiguous layers, the ambiguous layers will be classified whether they are AT layers or ATT layers. The ambiguous layers are labeled. In order to distinguish AT and ATT layers from each other, the local roughness [2] can be used. However, the distribution of the local roughness response does not spread well as shown in Fig. 4.5(c). To increase the distribution, the modification local roughness response is proposed. The labeled layers will be used with the modified local roughness which can be approximated as follows:

$$\bar{R}(\mathbf{x}) = \sum_{i=2}^{12} \psi_i(\mathbf{x}), \quad (4.5)$$

where $\psi_i(\mathbf{x}) = |CV_{\sigma_i}(\mathbf{x}) - CV_{\sigma_{i-1}}(\mathbf{x})|$ is the absolute of the difference between curvature with σ_i and curvature with σ_{i-1} , $CV_{\sigma_i}(\mathbf{x}) = \sqrt{\frac{1}{2}(\kappa_1^{\sigma_i}(\mathbf{x})^2 + \kappa_2^{\sigma_i}(\mathbf{x})^2)}$, $\kappa_1^{\sigma_i}(\mathbf{x})$, and $\kappa_2^{\sigma_i}(\mathbf{x})$ are the minimum and maximum curvatures at σ_i , respectively. According to the variation of the modified local roughness from different CTC data, the range of the modified local roughness response \bar{R} is normalizes as follows:

$$\mathcal{R}(\mathbf{x}) = 1.0 - \tan^{-1}(\bar{R}(\mathbf{x})) / \left(\frac{1}{2}\pi\right) \quad (4.6)$$

where $\mathcal{R}(\mathbf{x})$ is the modified local roughness response as shown in Fig. 4.5(d). To obtained AT layers, some of labeled layers are removed from the ambiguous layers. Thus, the remaining of ambiguous layers are AT layers. The labeled layers will be remained if any one of their voxels, \mathbf{x} , satisfies all of the following five conditions:

1. \mathbf{x} is on labeled layers.
2. There is at least one of air voxel in 4-neighbor of \mathbf{x} .
3. There is at least one of FTM voxel in 4-neighbor of \mathbf{x} .
4. The modified local roughness response $\mathcal{R}(\mathbf{x}) \leq t_{\mathcal{R}}$ where $t_{\mathcal{R}}$ is obtained from Otsu's method [18]. The inputs of Otsu's method [18] are all the modified local roughness response of points on labeled layers.
5. There is at least one voxel in 4-neighbor of $\mathcal{R}(\mathbf{x})$ that is also less than or equal to $t_{\mathcal{R}}$

At this step, AT layers can be distinguished from ATT layers. Thus, AT layers can be detected and be included within colonic lumen in order to be removed by EC method.

4.1.6 The proposed EC method

Before performing the EC method, FTM voxels are detected from \tilde{I} using simple threshold which is 200 HU. Thus, the location of voxels with CT number higher than 200 HU are the location of FTM voxels. Again, the binary image is used to represent the

location of the volume of interest. Let B_{colon} be the binary image that represents colonic lumen which consists of the binary image of air B_{air} , binary image of dilated AT layers $B_{AT_{dilate}}$ and binary image of FTM B_{FTM} such that $B_{colon} = B_{AT_{dilate}} \vee B_{air} \vee B_{FTM}$ where $B_{AT_{dilate}}$ is the morphological dilation with 26 neighbor structure element of AT layer, and \vee is the logical OR operation of binary images. There can be the AT layer remaining in EC result as shown in Fig. 4.6(b). In order to prevent to have the AT layer remaining, the hole filling operation is applied on B_{colon} where the AT layer remaining can present if there are holes in B_{colon} . So far, all voxels, which belong to colonic bowel, are obtained. The CT numbers of voxels in location of colonic bowel B_{colon} are changed using $\text{rand}(-1024, -900)$ where $\text{rand}(-1024, -900)$ is randomly chosen between -1024 and 900 which is experimentally similar to CT number of air.

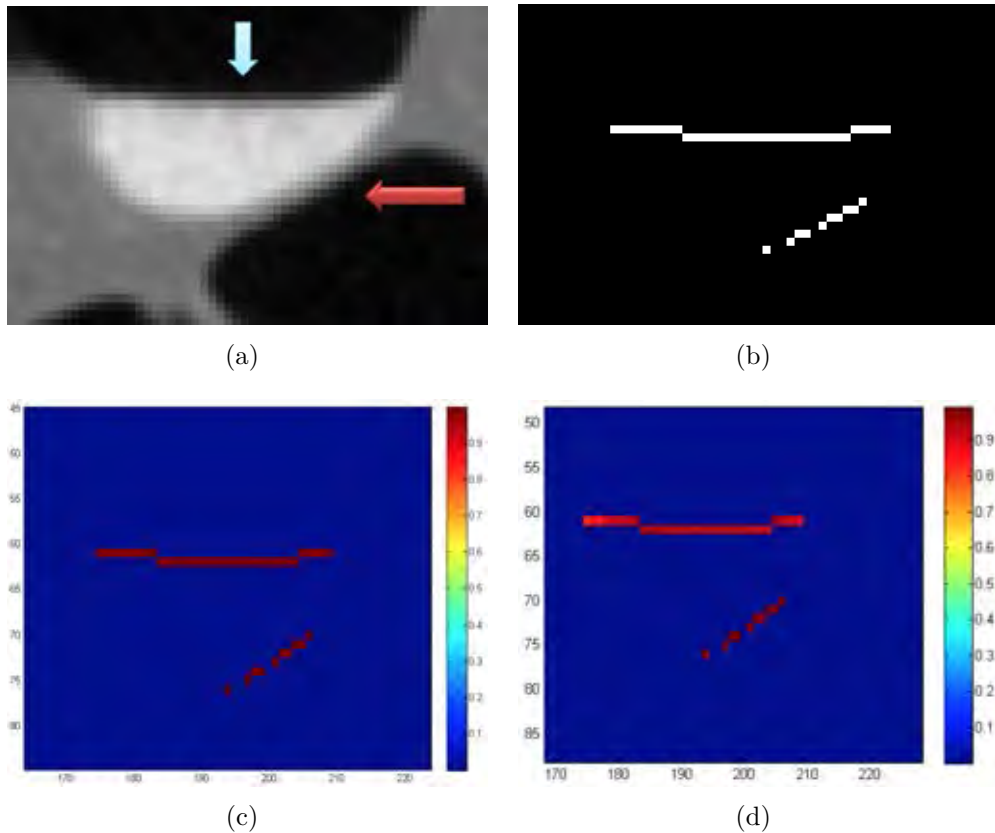


Figure 4.5: The regions of interest (ROI) of the ambiguous layers (a) The blue arrow points at AT layer and the red arrow points at ATT layer (b) The binary image represents the location of ambiguous layers (c) The result from ambiguous layer thinning (d) The result from using the local roughness [2] (e) The result from using the modified local roughness in (4.5)

4.1.7 Colonic lumen enhancement

The Gaussian smooth filtering with $\sigma = 0.5$ is applied to the voxels of colonic bowel in order to smooth edge between air and colonic wall as shown in Fig. 4.6(c).

After performing the proposed EC method, the submerged folds and polyps are preserved using the proposed PEH correction method. The AT layers are distinguished using the modification local roughness with layer labeling. Thus, the ATT layers are preserved from EC removal. However, the artifacts at three materials junction have not been solved yet. The following proposed EC methods will solve the artifacts at three materials junction, the similarity of AT and ATT layers, and PEH problem.

4.2 The second proposed EC method

4.2.1 AT layer identification

For the second proposed EC method, it is initially using the ambiguous layers from the our previous proposed EC method as shown in Figs. 4.8(a) and 4.8(b). In Figs. 4.8(a), the yellow dash circle surrounds a FTM region where the red arrow points at ATT layer, while the blue arrow points at AT layer. For the proposed AT layer detection, it can detect from the ambiguous layers using the number of connectivity from voxels of ambiguous layers to voxels of FTM in leaping distance [10] size 5. The ambiguous layers

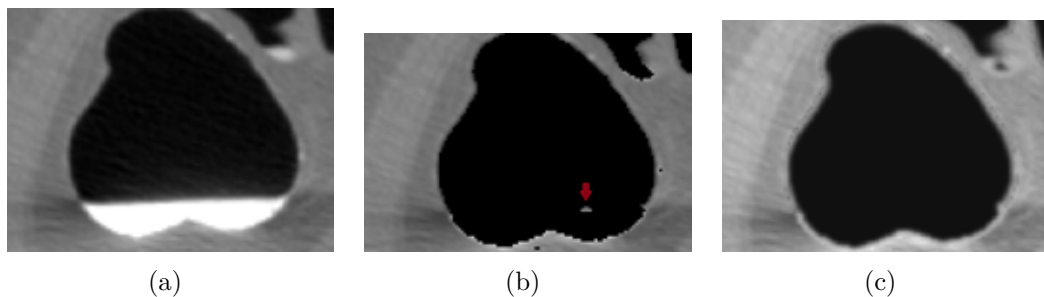
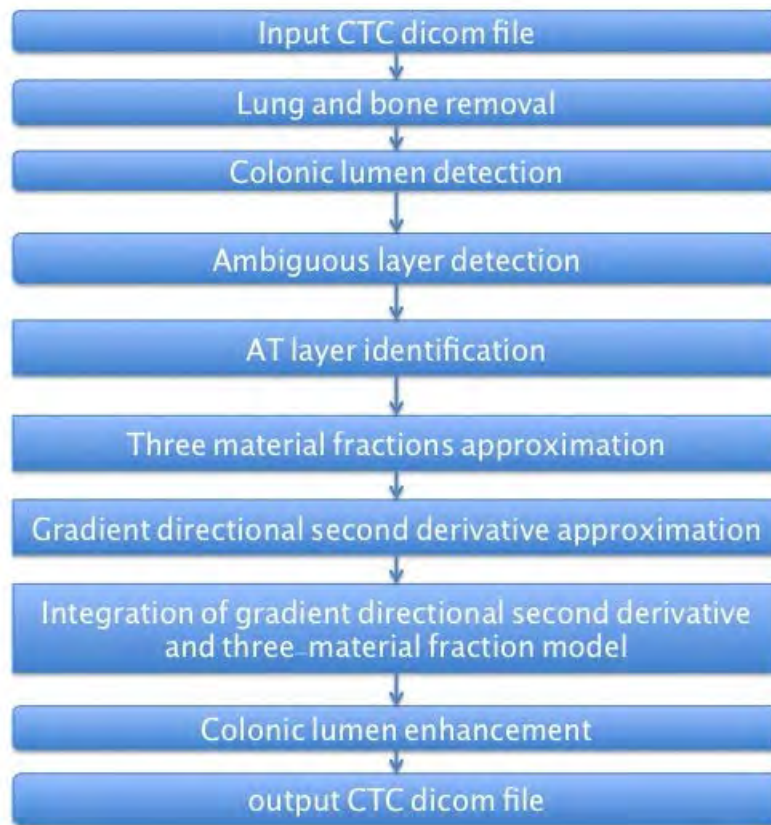


Figure 4.6: EC final result of the first proposed EC method (a) a ROI CTC image for illustrating hole filling operation (b) the floating artifact voxel and stair step edge (c) EC final result after applying hole filling operation the floating artifact voxel disappear and blurring the stair step effect



(a)

Figure 4.7: The second proposed EC process

around a FTM is used to count the connectivity in three directions which are left, right and downward directions. The algorithm 1 is used to detect AT layers around i^{th} FTM from j^{th} ambiguous layers where the algorithm 2 is used to count the connectivity from voxels of j^{th} ambiguous layers to voxels of i^{th} FTM. The algorithm 1 detects AT layers by removing some of ambiguous layers around i^{th} FTM where the remaining layers are AT layers. The left and right directions are called side direction. The algorithm 1 based on the assumption that the AT layer normally lies above the FTM where ATT layer are around the bend of a tagged pool where the CT scanner table lies at the bottom of CTC image. The number of connectivity is counted when the location of voxel of j^{th} ambiguous layers can leap into the location of voxel of i^{th} FTM. If a direction is in three directions and can make the connection, the connectivity of that direction is counted. Thus, for AT layers, there are number of connectivity from downward direction more than the connectivity

from side direction. In contrast, for ATT layers, there are number of connectivity from side direction more than connectivity from downward direction.

Algorithm 1: AT layer identification algorithm

```

input : region of  $i^{th}$  FTM and its labeled ambiguous layer
output: AT layer
1 for  $j \leftarrow a$  to  $b$  do
2   forall the  $v(x, y)$  in  $j^{th}$  ambiguous layer do
3     [left, right, down] = ConnectivityCounting( $x, y, FTM_i$ );
4     countLeft  $\leftarrow$  countLeft + left; countRight  $\leftarrow$  countRight + right;
5     countDown  $\leftarrow$  countDown + down;
6   end
7   total  $\leftarrow$  countLeft + countRight + countDown;
8   if total  $> 0$  then
9     if countLeft  $>$  countRight then
10      sideRatio  $\leftarrow$  countLeft/total;
11    else
12      sideRatio  $\leftarrow$  countRight/total;
13    end
14    downRatio  $\leftarrow$  countDown/total;
15    if sideRatio  $>$  downRatio then
16      forall the  $v(x, y)$  in  $j^{th}$  label do
17        | remove  $v(x, y)$  in  $j^{th}$  label
18      end
19    end
20  end
21 end

```

After obtained the AT layers from the algorithm 1 as shown in Figs. 4.8(c) and 4.8(d), the boundary between ST and FTM can be obtained by subtracting the AT layers from the boundary of FTM. The remaining of subtraction is the boundary between ST and FTM. The boundary between ST and FTM is called STT layer where ATT layers are in STT layers as shown in Fig. 4.8(d) and 4.8(e).

4.2.2 Three material fractions approximation

From the material fraction model in chapter III, material fractions of material transition between two materials can be obtained by applying the orthogonal projection of measure data $(I, \theta \sigma_w I_w)$ onto the arch function as shown in Fig. 4.9. The measure data $(I, \theta \sigma_w I_w)$ of voxels in AT layers can be used to find bases of material transition

Algorithm 2: connectivity counting

input : coordinate (x, y) of j^{th} ambiguous layer and voxels in i^{th} FTM
output: the number of connectivity from j^{th} ambiguous to i^{th} FTM in three directions

```

1 for  $k \leftarrow 1$  to 5 do
2   | if  $(x - k, y)$  is in  $i^{th}$  FTM then // count the connectivity of
   | voxels in  $j^{th}$  ambiguous layer to  $i^{th}$  FTM in left direction
3   | | countLeft  $\leftarrow$  countLeft + 1;
4   | | break;
5   | end
6 end
7 for  $k \leftarrow 1$  to 5 do
8   | if  $(x + k, y)$  is in  $i^{th}$  FTM then // count the connectivity of
   | voxels in  $j^{th}$  ambiguous layer to  $i^{th}$  FTM in right direction
9   | | countRight  $\leftarrow$  countRight + 1;
10  | | break;
11  | end
12 end
13 for  $k \leftarrow 1$  to 5 do
14  | if  $(x, y + k)$  is in  $i^{th}$  FTM then // count the connectivity of
   | voxels in  $j^{th}$  ambiguous layer to  $i^{th}$  FTM in downward
   | direction
15  | | countDown  $\leftarrow$  countDown + 1;
16  | | break;
17  | end
18 end

```

between air and FTM while the measure data $(I, \theta \sigma_w I_w)$ of voxels in STT layers can be used to find bases of material transition between ST and FTM where the bases of material transition between air and ST can be used from the previous two transition. All bases from three material transitions can be used to form a triangle. Since obtained three vertices of triangles, three material fractions can be obtained. Let

- t_{LTT} and t_{HTT} be material fractions from material transition of ST and FTM,

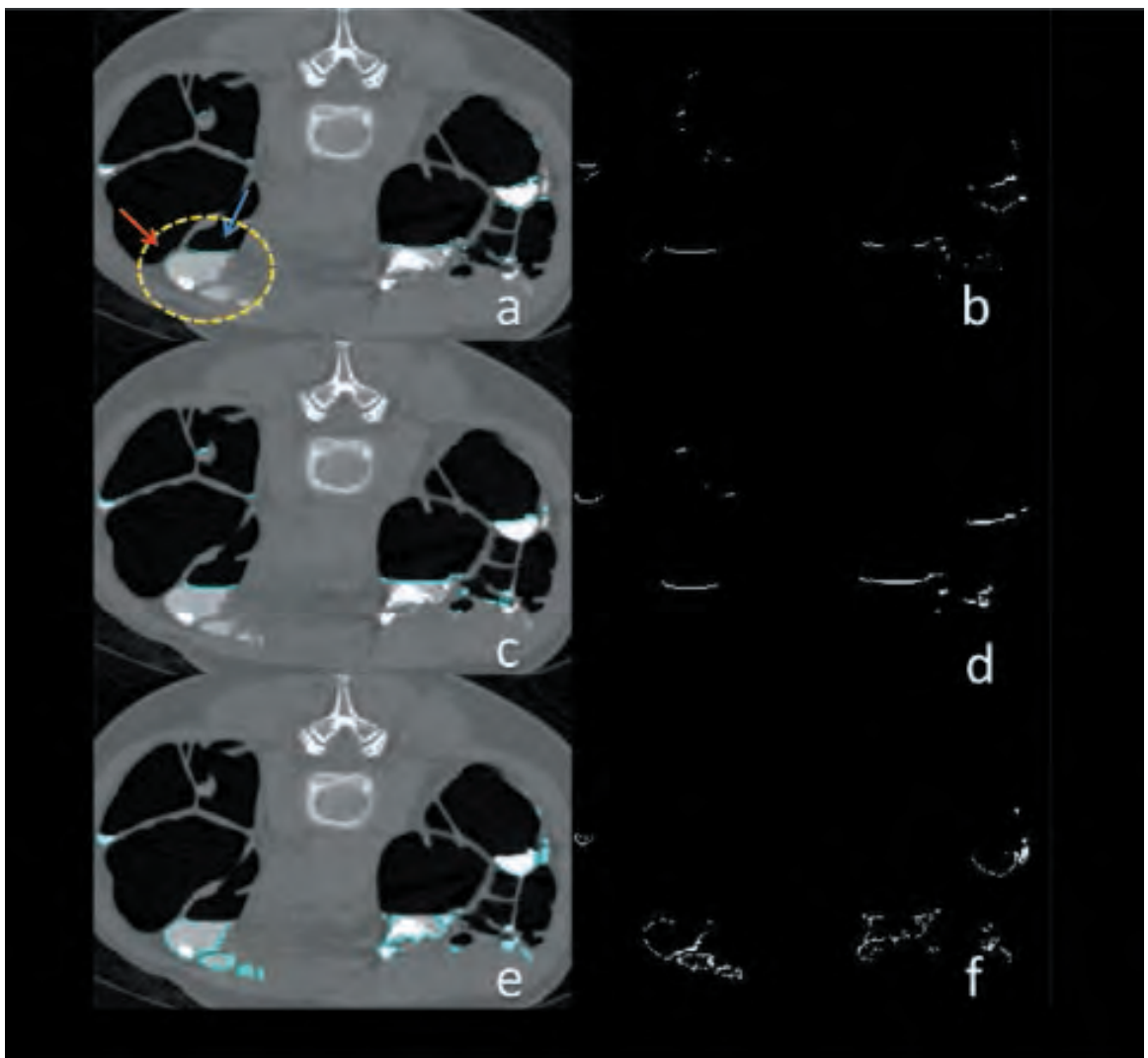


Figure 4.8: Result of Ambiguous layer detection, AT layer identification and STT layer detection (a) CTC image with the ambiguous layers (b) the ambiguous layers in binary image (c) CTC image with AT layer (d) AT layer in binary image (e) CTC image with STT layer (f) STT layer in binary image

- $t_{L_{TA}}$ and $t_{H_{TA}}$ be material fractions from material transition of air and FTM,
- $t_{L_{SA}}$ and $t_{H_{SA}}$ be material fractions from material transition of ST and air,
- L_{TT} and H_{TT} be pure material CT number bases of ST and FTM, respectively,
- L_{TA} and H_{TA} be pure material CT number bases of air and FTM, respectively,
- L_{SA} and H_{SA} be pure material CT number bases of ST and air, respectively.

Thus, the material fractions of air, ST, and FTM at three materials junction can be approximated as follows:

$$\begin{aligned}
 t_{air} &= \frac{t_{L_{SA}} + t_{L_{TA}}}{3}, \\
 t_{ST} &= \frac{t_{H_{SA}} + t_{L_{TT}}}{3}, \\
 t_{FTM} &= \frac{t_{H_{TA}} + t_{H_{TT}}}{3} = 1 - t_{air} - t_{ST},
 \end{aligned} \tag{4.7}$$

where t_{air} , t_{ST} , and t_{FTM} are material fractions of air, ST and FTM, respectively.

4.2.3 Integration of gradient directional second derivative and three-material fraction model

In order to aware of PEH ST voxels removal from EC method, the only linear combination of material fraction model cannot transform the CT number of PEH ST voxels into ST range correctly. Thus, for the CT numbers between ST and FTM, the GDSD are integrated into material fractions of material transition between ST and FTM in the same manner in (3.19) as follows:

$$I_{peh} = t_{L_{TT}} \cdot L_{TT} + t_{H_{TT}} \cdot \{f_{nn} \cdot L_{TA} + (1 - f_{nn}) \cdot H_{TA}\}, \tag{4.8}$$

where I_{peh} are new CT number of voxels in STT layers and FTM. By applying (4.8), the PEH CT numbers of voxels in ST can be reduced into ST range and the CT numbers of FTM voxels are transformed into the CT numbers of air instead.

In colonic bowel, although the CT numbers of FTM and STT layers are transformed but there also are the CT numbers of voxels in AT layers and artifacts at three materials junction that need to be changed. Therefore, the CT numbers of voxels in AT layers and artifacts at three materials junction are transformed as follows:

$$I_{T_{junction}} = t_{air} \cdot L_{TA} + t_{ST} \cdot L_{TT} + t_{TR} \cdot L_{TA}, \quad (4.9)$$

where $I_{T_{junction}}$ are new CT number of voxels at location AT layers and artifacts at three materials junctions.

In the conclusion of the proposed EC method, the GSD are mainly used to detect ST in vicinity of FTM or are integrated into material fraction model in order to

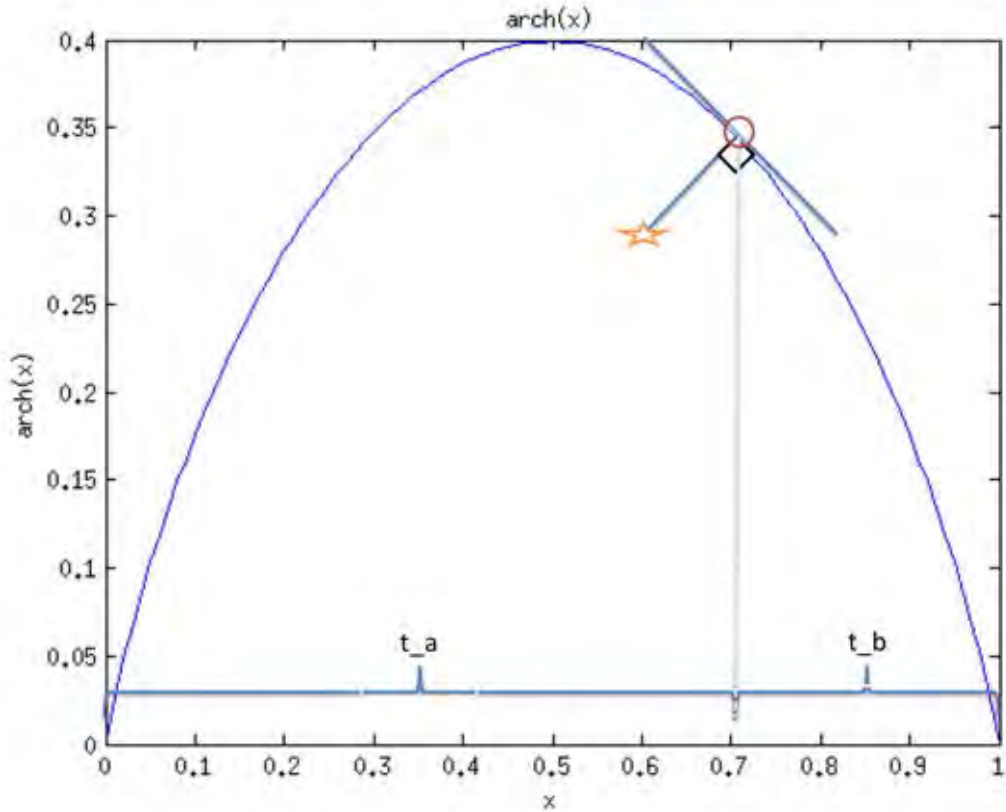


Figure 4.9: $\{I, \theta_{\sigma_{\omega}} I_{\omega}\}$ is represented by star. $\{I', \theta_{\sigma_{\omega}} I'_{\omega}\}$ is the red circle on $arch(I')$. The red circle is the intersection point of orthogonal line to tangent line of $arch(x)$. $(I', \theta_{\sigma_{\omega}} I'_{\omega})$ on $arch(I')$ is used to find material fraction.

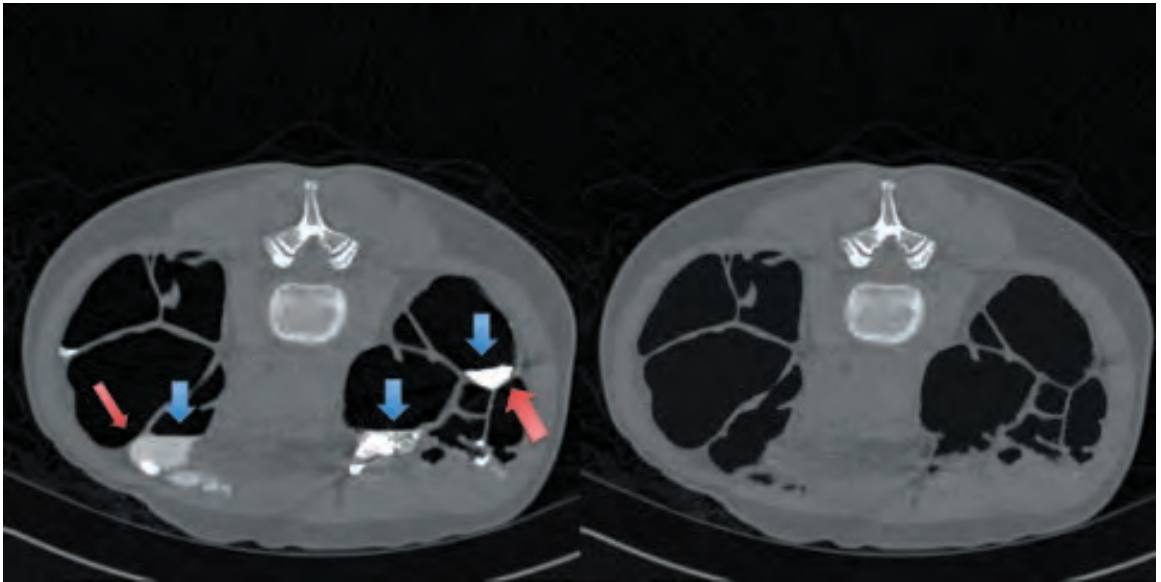


Figure 4.10: a result of the second proposed EC method (a) the CTC image Blue arrows point at AT layers that are removed at the same time as FTM Red arrows point at ATT layers that are preserved from EC (b) the axial final result from our second proposed method

preserve ST component with PEH effect from EC method removal. The modification of local roughness are proposed in order to increase the distribution from the existing local roughness. The increasing of the distribution of the modification local roughness can help to distinguish AT layers from ATT layers easier. Unfortunately, the high computation of the modification local roughness is the same as the existing local roughness. Therefore, the AT layer detection is proposed in order to reduce computational time from the modification of local roughness. After obtaining AT layers, the ATT layers are preserved from EC removal. Finally, the last proposed EC method has solved the PEH problem, the similarity of AT layers and ATT layers, the artifacts at three materials junctions. The CT numbers of PEH ST voxels is reduced into ST range to preserve ST component, especially, polyps and folds from erroneous EC removal. The AT layers, known as PV effect layers, and artifacts at three materials junctions are removed simultaneously as shown in Fig. 4.10.

CHAPTER V

EXPERIMENTAL RESULTS AND CONCLUSION

Since there are two proposed EC methods, there are two EC results. The first proposed EC method consists of GDSD, PEH CT number linear transformation and the modified local roughness. The second proposed EC method consists of AT layer identification and integration of GDSD and material fraction model. The first EC results come from the first proposed EC method. The second EC results come from the second proposed EC method.

5.1 The first proposed EC method evaluation

5.1.1 CTC data set detail

The first proposed EC method used three data sets of CTC images. The first CTC data set came from Pickhardt *et al.* [19]. The second CTC data set came from King Chulalongkorn Memorial Hospital. The first and the second CTC data sets are used as the test sets. The last data set came from the Philips CT scanner, Brilliance 64, is used as the training set.

Eighteen cases are randomly selected from the first CTC data set and are used in objective evaluation. Both supine and prone positions were acquired using multi-detector CT scanning with four or eight channel CT scanner of 1.25 mm or 2.5 mm collimation using the table speed of 15 mm/s and the reconstruction interval is 1 mm.

Four cases are randomly selected from the second CTC data set and are used in subjective evaluation. Both supine and prone positions are acquired using GE medical System with slice thickness less than 1.25 mm, spacing between slices less than 1 mm,

Table 5.1: Grading scheme in cleansing quality evaluation

Inadequate	Moderate	Good	Excellent
10/105	30/105	60/105	5/105
9.52%	28.57%	57.14%	4.76%

Table 5.2: Five causes for low quality EC

T-junction	Inhomo	Collapsed	Noise	Incomplete
100/105	10/105	0/105	0/105	0/105
95.24%	9.52%	0%	0%	0%

230 mA X-ray tube current, and a voltage of 120 kVp.

The last CTC data set is acquired with patient preparation as Pickhardt *et al.* [19] did with parameters: 0.9 mm slice thickness, 0.7 mm spacing between slices, 197mA X-ray tube current and a voltage of 120 kVp.

5.1.2 Clinical evaluation

The subjective evaluation is used to perform clinical evaluation. The subjective evaluation uses four grades of cleansing quality with five causes of low quality [10]. The four grades of cleansing quality with five causes of low quality are determined by the experienced radiologist from King Chulalongkorn Memorial hospital. Four grades of cleansing quality consist of excellent, good, moderate and inadequate. Five causes of low quality consist of artifacts at T-junction, inhomogeneous tagging, collapsed area, image noise and incomplete EC. The excellent quality is given if and only if there is no cause of low quality. The inadequate quality is given if and only if there are artifacts and incomplete cleansing. Thus, the cleansing quality of the complete cleansing could be evaluated as moderate, good, excellent which depends on radiologist's opinion. The completeness of cleansing was evaluated from axial view while the cleansing quality was evaluated from the panoramic endoluminal view, called band view [10] from Vitrea software of Toshiba CT scanner as shown in Fig. 5.1 and 5.2. In Fig. 5.1 and 5.2, the axial views are the first row while the rest are the band view. The partially and completely submerged polyps can be revealed after applying the first proposed EC method.

For 105 band view images of CTC data from King Chulalongkorn memorial hospital, the average grade that was given by the radiologist is 2.5714 out of 4. Among of the cleansing results, 4.76% receive excellent quality, 57.14% receive good quality, 28.57% receive moderate quality and 9.52% receive inadequate quality for both artifacts at T-junction and incomplete cleansing due to inhomogeneous tagging. The artifact at T-junction is the main cause of low quality for every case while the second cause comes from inhomogeneous tagging. However, the artifacts at T-junctions beyond the scope of the first proposed EC method.

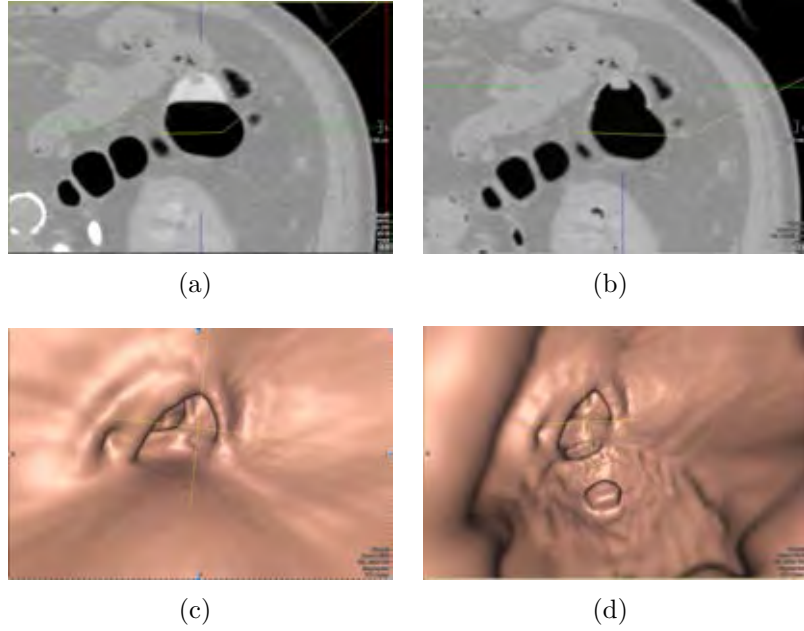


Figure 5.1: The first row contains region of interest (ROI). The second row contains volume of interest (VOI) of the first row. (a) ROI of a CTC image (b) ROI of EC of a CTC image (c) VOI of a CTC image (d) VOI of EC of a CTC image

5.1.3 PEH correction Evaluation

Since the first proposed EC method consists of GDSD and the PEH CT number linear transform, the PEH correction evaluation is one of the objective evaluations that needs to be performed. The ADC method [15] is used to compare with the proposed PEH correction method. The main parameters σ_1 and σ_2 are calculated from the following equations:

$$\sigma_1(v_q) = 0.0001v_q + 0.392 \quad (5.1)$$

and

$$\sigma_2(r) = -0.0007r + 0.59. \quad (5.2)$$

For the results from ADC method, there is no result for the case of PEH ST voxels with CT numbers higher than 500 HU. Figures. 5.3(a), 5.4(a) and 5.5(a) show regions of interest (ROIs) with CT numbers as high as 500 HU due to PEH effect. Figures. 5.3(b), 5.4(b) and 5.5(b) show ROIs of the results from ADC method. Figures. 5.3(c), 5.4(c) and 5.5(c) show ROIs of the results from the proposed PEH correction method. Figure. 5.3(d), 5.4(d) and 5.5(d) show CT numbers profiles where

- the red lines represent CT numbers of the red dots in Figs. 5.3(a), 5.4(a) and 5.5(a), respectively.
- The blue lines represent CT numbers of the blue dots in Figs. 5.3(b), 5.4(b) and 5.5(b), respectively.

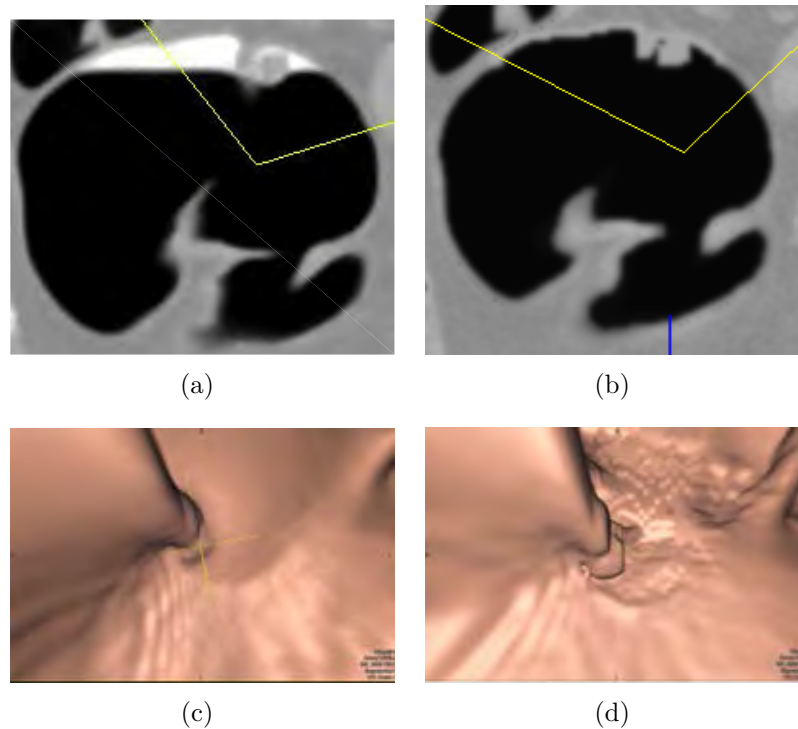


Figure 5.2: The first row contains ROI. The second row contains VOI of the first row. (a) ROI of a CTC image (b) ROI of EC of a CTC image (c) VOI of a CTC image (d) VOI of EC of a CTC image

- The magenta lines represent CT numbers of the magenta dots in Figs. 5.3(c), 5.4(c) and 5.5(c), respectively.

Figures. 5.3, 5.4 and 5.5 illustrate that the proposed PEH correction method can reduce CT numbers of PEH ST voxels, which can be as high as 500 HU, while the ADC method fails in this case. For the blue lines in Figs. 5.3, 5.4 and 5.5, the proposed PEH correction method can reduce CT numbers of PEH ST voxels to be lower than the maximum CT number of ST which is 100 HU. For the magenta line in Figs. 5.3(d), 5.4(d), and 5.5(d), the ADC method cannot reduce CT numbers of PEH ST voxels to be lower than the maximum CT number of ST.

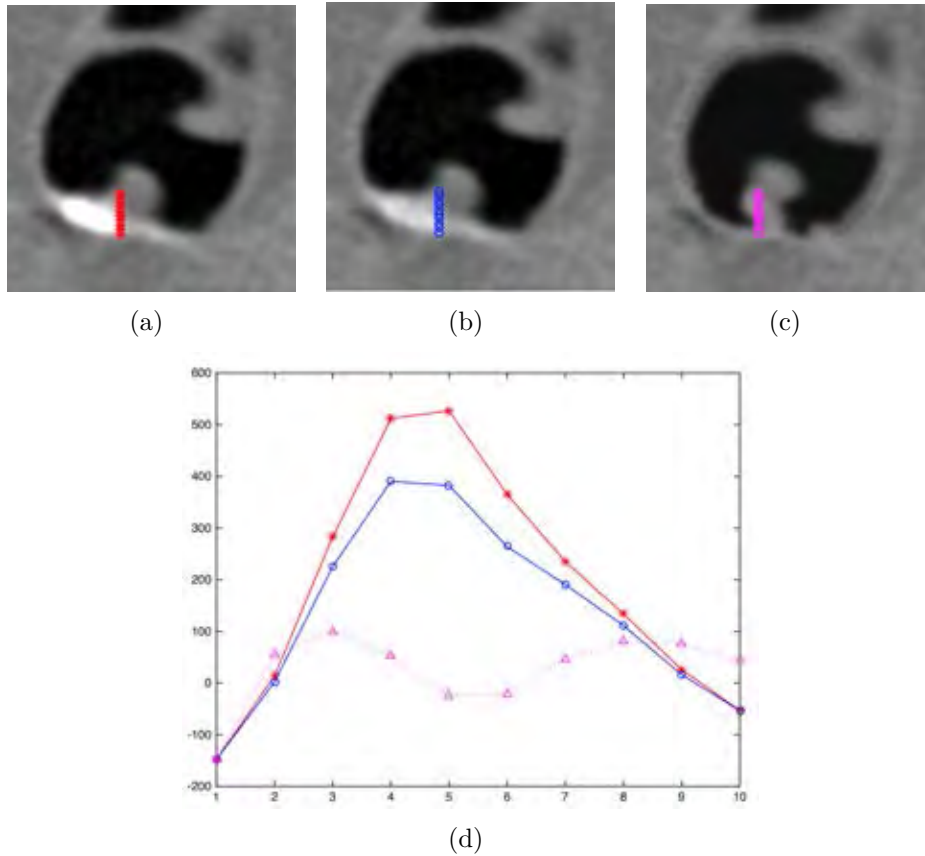


Figure 5.3: CT number profile of a submerged fold (a) ROI of a CTC image (b) ROI from ADC result (c) ROI from our first proposed EC (d) profile of CT numbers where y -axis represents CT number and x -axis represents location of pixel in ROI image

5.1.4 Objective Evaluation

To evaluate the benefit of the proposed PEH correction method, the second CTC data from Pickhardt *et al.* is used. The 974 ROIs are selected which contain polyps and folds. The ground truth of FTM regions in 974 ROIs are made without including the location of polyps, folds and with including the location of AT layers. The locations of FTM regions in the ground truth are presented in binary images. The ground truth data set is verified by the radiologist. Figure. 5.6(a) shows a CTC image with ROIs at marked by a green rectangle. Figure. 5.6(b) shows the ground truth with location of FTM (white pixels). Figure. 5.6(c) shows the labels of FTM regions in the ground truth. Figure. 5.6(d) shows the labels of FTM regions obtained from the first proposed EC method. In order to perform the quantitative EC evaluation, the difference of the regions with the

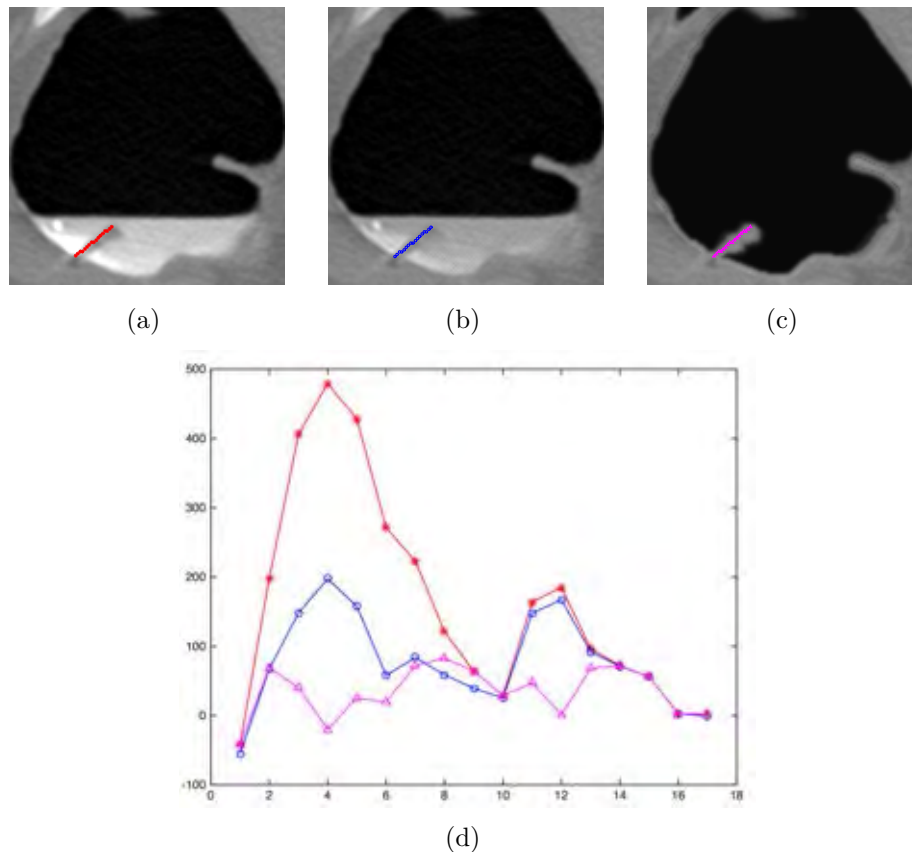


Figure 5.4: CT number profile of a submerged fold (a) ROI of a CTC image (b) ROI from ADC result (c) ROI from our first proposed EC (d) profile of CT numbers where y -axis represents CT number and x -axis represents location of pixel in ROI image

same label between the ground truth and the results from the first proposed EC method were compared. The comparison uses the exclusive-OR (XOR) operation to determine the difference. The difference is used to calculate the mean relative error which was further used to calculate the global mean relative error, \mathcal{S} , as follows:

$$\mathcal{S} = \left(\frac{1}{\sum_i \mathcal{N}(\mathcal{U}_i)} \sum_i \left(\mathcal{N}(\mathcal{U}_i) \times \frac{\mathcal{N}(\mathcal{U}_i \oplus \mathcal{V}_i)}{\sum_i \mathcal{N}(\mathcal{U}_i)} \right) \right) \times 100, \quad (5.3)$$

where \oplus is the XOR operation between two regions with the same label in two binary images, \mathcal{U}_i is the i^{th} ROI of the ground truth, \mathcal{V}_i is the i^{th} ROI of the results from the first proposed EC method and $\mathcal{N}(\cdot)$ is the number of white pixels in the i^{th} ROI. For each

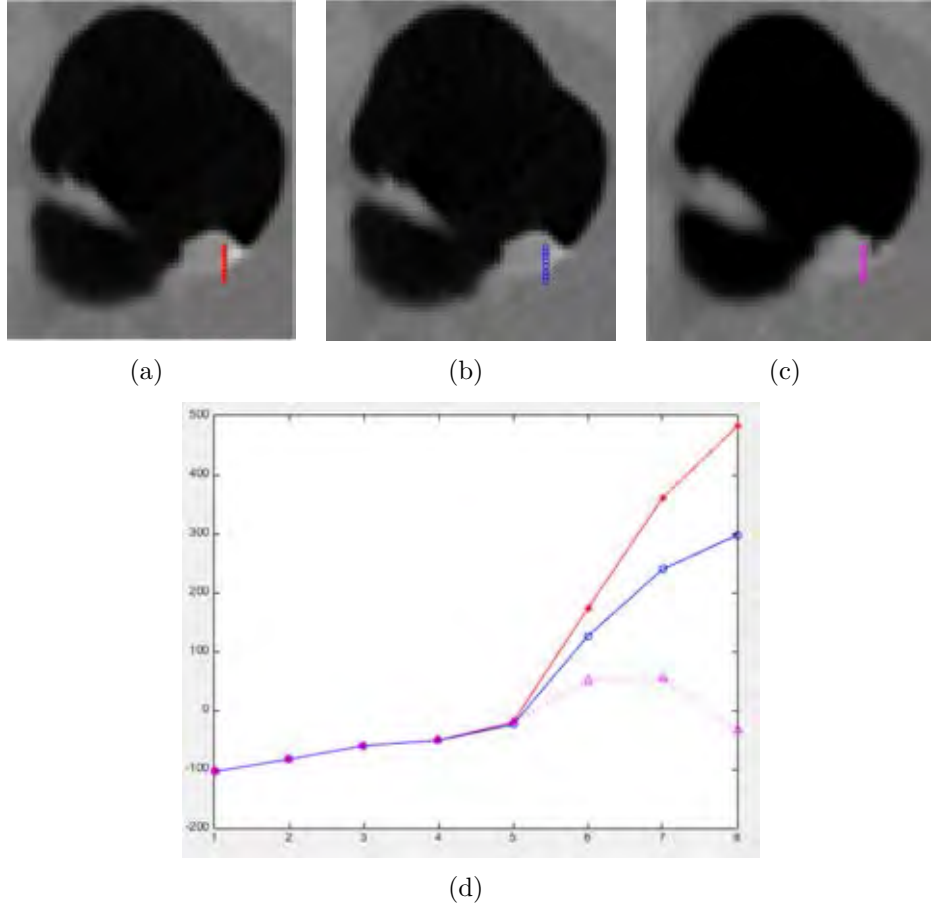


Figure 5.5: CT number profile of pedunculate polyp. (a) ROI of a CTC image (b) ROI from ADC result (c) ROI from our first proposed EC (d) profile of CT numbers where y -axis represents CT number and x -axis represents sample pixels from (a), (b) and (c)

individual i^{th} region, the number of white pixels is not equal. Therefore, the weight for each i^{th} region must be used in order to indicate the influence to the total of the global mean relative error.

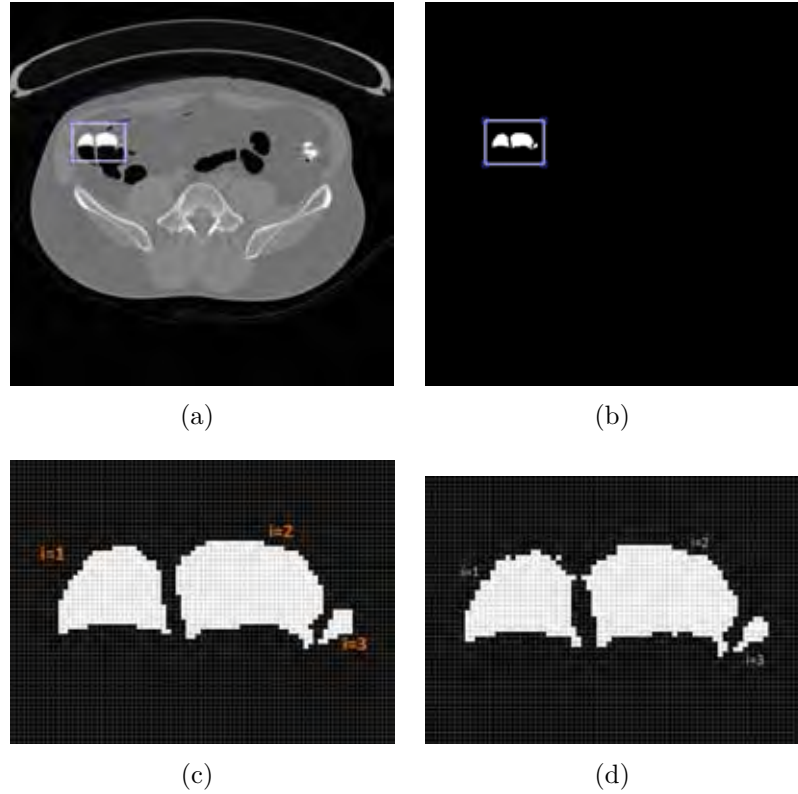


Figure 5.6: The comparison process between binary image of ground truth and the results of the first proposed EC method (a) A sample CTC image with ROIs in the small rectangle (b) A binary image of the ground truth with ROIs in the small rectangle (c) Labeled ROIs of the ground truth (d) Labeled ROIs of the result at the same position as the ground truth

To evaluate goodness of cleansing, the global mean relative error from 974 ROIs was used. The global mean relative error is approximately 0.01%. Thus, the goodness of cleansing of the results is about 99.99%, while the z-test shows that the global mean relative error from the first proposed EC method is less than 0.016% with 99.99% confidence.

For fold preservation, CT numbers of the submerged folds are further determined. CT numbers of the submerged folds are divided into four intervals as shown in Table. 5.3. All selected submerged folds that is used in Table. 5.3 are preserved even though the CT

Table 5.3: Numbers of the remaining per the existing of submerged folds in four intervals.

interval of CT number	number of fold
200 – 300	15/15
300 – 400	10/10
400 – 500	13/13
≥ 500	2/2

numbers are equal to or greater than 500 HU.

Table 5.4: The numbers of actual polyps from CTC data of King Chulalongkorn Memorial Hospital.

case	outstanding	partial	complete
1 supine	1	1	-
1 prone	1	-	1
2 supine	4	1	-
2 prone	3	1	1
3 supine	1	-	-
3 prone	1	-	1
4 supine	1	1	-
4 prone	1	1	-

For polyps detection, there are 19 polyps in both supine and prone positions in CTC data from King Chulalongkorn Memorial hospital as shown in Table 5.4 where the outstanding polyps (outstanding) are the polyp without lying against FTM, the partial submerged polyps (partial) are the polyp that is partially covered by FTM and the complete submerged polyps (complete) are the polyp that is complete covered by FTM. There are 5 partially submerged polyps, 3 completely submerged polyps, and the rest 13 polyps are outstanding from FTM. For partially and completely submerged polyps, all of them still exist after applying the first proposed EC method.

5.1.5 Visual Assessment

Next, the proposed modified local roughness is used to preserved ATT layers as shown in Fig. 5.7. Fig. 5.7(a) shows an ATT layer which is pointed by the red arrow. The AT layer is pointed by the blue arrow, while a small rectangle pointed by the red arrow contains an ATT layer as shown in Fig. 5.7(b). Fig. 5.7(c) shows the ambiguity

between an AT layer and an ATT layer after FTM removal. Since the first proposed EC method consists of the AT layer segmentation, an AT layer is removed while an ATT layer is preserved correctly as shown in Fig. 5.7(d). Fig. 5.7(e) shows the VOI of Fig. 5.7(b) which contains the volume of water. Fig. 5.7(f) shows VOI of Fig. 5.7(d) which contains the preserved ATT layer.

For inhomogeneous FTM (IFTM) cases, some of CTC data from Pickhardt *et al.* [19] contain IFTM in colonic bowel where the content of IFTM is not homogeneous as shown in Figs. 5.8(a) and 5.8(c). This inhomogeneity can lead to erroneous EC results where the results are not completely cleansed because CT numbers of some voxels in IFTM is in ST range. If these voxels does not attach to colonic wall, then they can be removed using hole filling operation presented in the first proposed EC method as shown

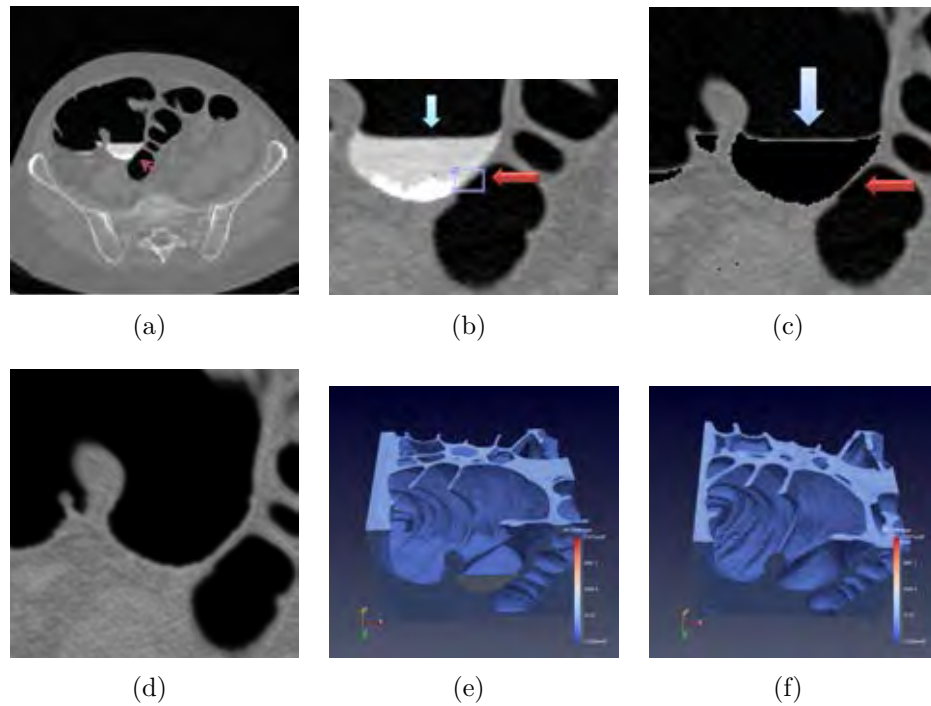


Figure 5.7: The comparison of axial view between the result using only thresholding and the result from the first proposed EC method is used. The comparison of VOI between a result with and without applying the first proposed EC method is used. (a) The ambiguous case (b) The blue arrow points at PVE between air and FTM components which is an AT layer and the red arrow points at the thin ST between air and FTM components which is an ATT layer (c) The remaining layers after FTM removal using threshold, 200 HU (d) ROI of our first proposed EC result (e) VOI of original CTC image volume (f) VOI of our first proposed EC result from using paraview software

in Figs. 5.8(b) and 5.8(d). In contrast, if these voxels attach to colonic wall, then the only hole filling operation cannot handle this case.

So far, the evaluation results assure reliability and efficiency to preserve PEH ST voxels, remove PV effect layers or AT layers and preserve ATT layers of the first proposed EC method. Next, the evaluation results of the second proposed EC method will be justified to illustrate the improvement from the first proposed EC method.

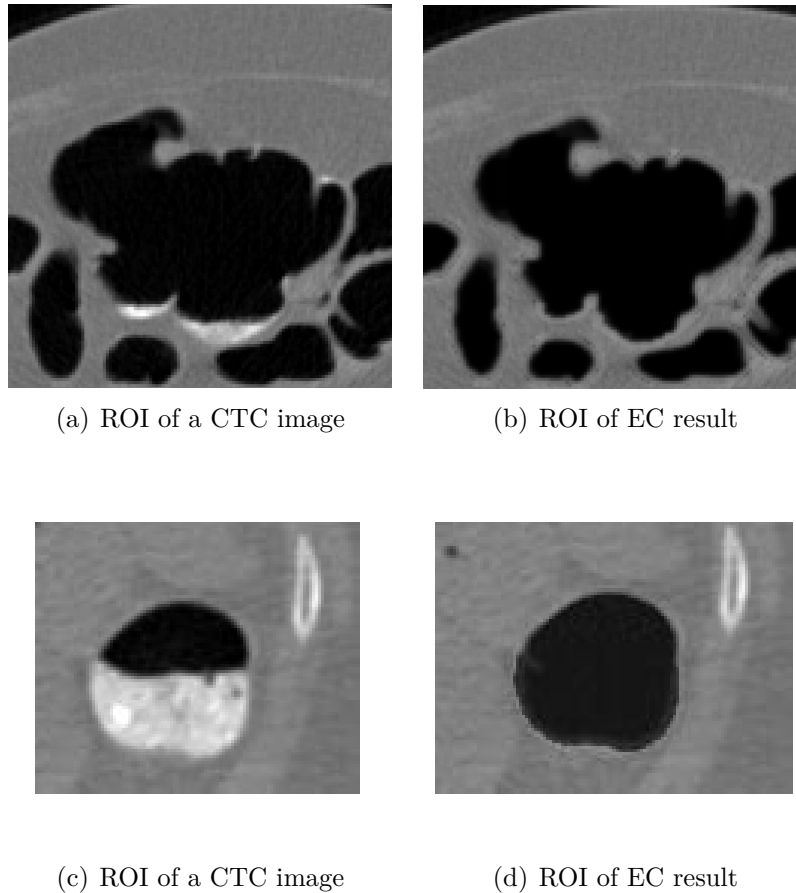


Figure 5.8: The first proposed EC method for IFTM case (a) The ambiguous case which contains both AT and ATT layers (b) FTM and AT layers were removed correctly and an ATT layer is preserved by our first proposed EC method (c) The IFTM case (d) The result after applying our first proposed EC to IFTM case

5.2 The second proposed EC method evaluation

5.2.1 CTC data set detail

CTC data from three different sources are used to evaluate of the second proposed EC method. For the first source, 5 cases from Pickhardt *et al.* [19] are used for testing set. For the second source, 10 cases from King Chulalongkorn Memorial Hospital are used for testing set. For the last source, a case obtained from Philips CT scanner, Brilliance 64, with the same preparation as CTC data used in Pickhardt *et al.* [19] is used for training set. All cases from three sources are acquired both supine and prone positions. Each scan of every case consists of approximately 600 consecutive CTC images of size 512×512 pixels with spatial resolution of approximately 0.66 mm in three dimensions.

5.2.2 Clinical evaluation

The clinical evaluation is performed using four levels of cleansing quality grading with five causes of low quality as before. To compare the preference between the remaining artifacts at T-junction of the results from the second proposed EC method EC_{prop} and the syngo.via client 3.0 software of Siemen CT scanner EC_{syngo} which is currently used at King Chulalongkorn Memorial Hospital. In order to illustrate the improvement from the existing method, EC_{prop} was compared with the existing EC method EC_{prev} from Lee *et al.* [11]. For the pictorial results, they are used to explain why the results from EC_{prop} improve from those of EC_{prev} or the results from EC_{prop} is more preferable than the results from EC_{syngo} . There are 467 band view images from the results of EC_{prop} , EC_{prev} , and the EC_{syngo} .

Table 5.5: Grading scheme in cleansing quality evaluation

Cleansing quality grade		
Inadequate	0/467	0.00%
Moderate	135/467	28.91%
Good	247/467	52.89%
Excellent	85/467	18.20%

For the first clinical evaluation, the completeness of cleansing is evaluated using

the axial view image while the quality of cleansing is evaluated using the 3D band view image by the opinion of the radiologist. The quality of cleansing uses four grades with five causes of low quality as before. From the clinical evaluation results shown in Table. 5.5, the average grade is 2.89 out of 4 where 18.20% of test data are graded as excellent, 52.89% of test data are graded as good, 28.91% of test data are graded as moderate, and none is graded as inadequate. Thus, all cases of E_{prop} are cleansed completely. However, the artifacts at T-junctions are generally given as a cause of low quality which is 69.81% where other causes of low quality are not given. The artifact at T-junction cause of low quality can only indicate the existing of the remaining of artifacts at T-junction but it cannot indicate the quantity of the remaining. Therefore, the quantity of the remaining of artifacts at T-junction are further investigated.

Table 5.6: Five causes for low quality EC

Reason for low quality EC		
Artifacts at T-junction	326/467	69.81%
Inhomogeneous tagging	0/467	0.00%
Collapsed area	0/467	0.00%
Image noise	0/467	0.00%
Incomplete EC	0/467	0.00%

To estimate the quantity of the remaining of artifacts at T-junction, the volume of the remaining of artifacts at T-junction is divided in 8 scales and approximated by the radiologist as shown in Table. 5.7. The description of scales are as follows: 0% remaining means the radiologist cannot identify the location of artifacts at T-junction at all or can easily say that the remaining of artifact at T-junction is invisible, which is the most general case, 1 – 99% remaining means the percentage of the remaining that can be seen by the radiologist and 100% remaining means that the artifact cannot be removed at all.

There are 30.19% of the test data that are identified as the 0% remaining. For the 1 – 50% remaining, there are 37.48% that are identified. For the 51 – 99% remaining, there are 19.27% that are identified. Thus, there are 86.94% of the test data that the radiologist cannot identify the location of artifacts at T-junctions completely. For the 100% remaining, there are only 13.06% that were identified and were further compared

with the results from EC_{syngo} as shown in Figs. 5.9 and 5.10. There are 9.21% of the results from EC_{prop} that are more preferable while there are 3.85% of the results from EC_{syngo} that are more preferable by the radiologist as shown in Table. 5.8 where the scale of preference 1, 2 and 3 mean slightly better, better and much better.

In Figs. 5.9 and 5.10, the artifacts at T-junctions were compared where (a) and (d) of Fig. 5.9 and 5.10 are the results from EC_{prop} where the artifacts at T-junction are invisible by radiologist opinion, (b) and (e) of Fig. 5.9 and 5.10 are the results from EC_{syngo} , and (c) and (f) of Fig. 5.9 and 5.10 are the original CTC images.

In Fig. 5.11, the submerged polyp under FTM are compared where (a) and (d) of Fig. 5.11 are the results from EC_{prop} , (b) and (e) of Fig. 5.9 are the results from EC_{syngo} where submerged polyp is disappeared, (c) and (f) of Fig. 5.9 are the original CTC images.

The last comparison between EC_{prop} and EC_{prev} is used to indicate the improvement of EC_{prop} from the existing method EC_{prev} [11] as shown in Figs. 5.12 and 5.13. The opinion of radiologist is used to evaluate the difference between two methods where the scales of preference -1 , -2 and -3 mean that EC_{prev} is slightly better, better and much better. In contrast, the scales of preference 1, 2 and 3 mean that EC_{prop} is slightly better, better, and much better. Scale 0 indicates that the results from two methods are similar.

Table 5.7: Volume of the remaining artifacts at T-junctions after applying EC_{prop}

	0%	1-10%	11-20%	21-30%	31-40%	41-50%	51-99%	100%
#	141/467	41/467	30/467	43/467	16/467	45/467	90/467	61/467
%	30.19%	8.78%	6.42%	9.21%	3.43%	9.64%	19.27%	13.06%

Table 5.8: Comparing the preference of the remaining artifacts at T-junctions after applying ECs between EC_{prop} and EC_{syngo}

	1	2	3	total
EC_{Syngo}	14	2	2	18/61(3.85% of 467)
EC_{Prop}	38	3	2	43/61(9.21% of 467)

Table 5.9: Comparison between the results from EC_{prop} and EC_{prev} [11]

EC quality comparison between EC_{prop} and EC_{prev}							
	-3	-2	-1	0	1	2	3
#	2/467	3/467	29/467	327/467	84/467	21/467	1/467
%	0.43%	0.64%	6.21%	70.02%	17.99%	4.50%	0.21%

The comparison results in Table. 5.9 shows that approximately 70% of EC_{prop} and EC_{prev} are similar while EC_{prop} gets slightly better scale for approximately 18% and EC_{prev} gets slightly better scale for approximately 6.21%. For better and much better scale of EC_{prop} , they receive 4.5% and 0.21%, respectively. For better and much better scale of EC_{prev} , they receive 0.64% and 0.43%, respectively.

The comparison results from EC_{prop} shows the improvement from EC_{prev} that comes from ATT layer preservation of the EC_{prop} as shown in Fig. 5.12. Figure. 5.12 shows that the ATT layers pointed by yellow arrow are preserved while the ATT layers pointed by red arrow in the results of EC_{prev} are disappeared. The damage of ATT layer disappearing may cause a hole in 3D band view from the erroneous EC method as shown in Fig. 5.13. For the degrees of fold preservation from EC_{prop} and EC_{prev} , Fig. 5.14

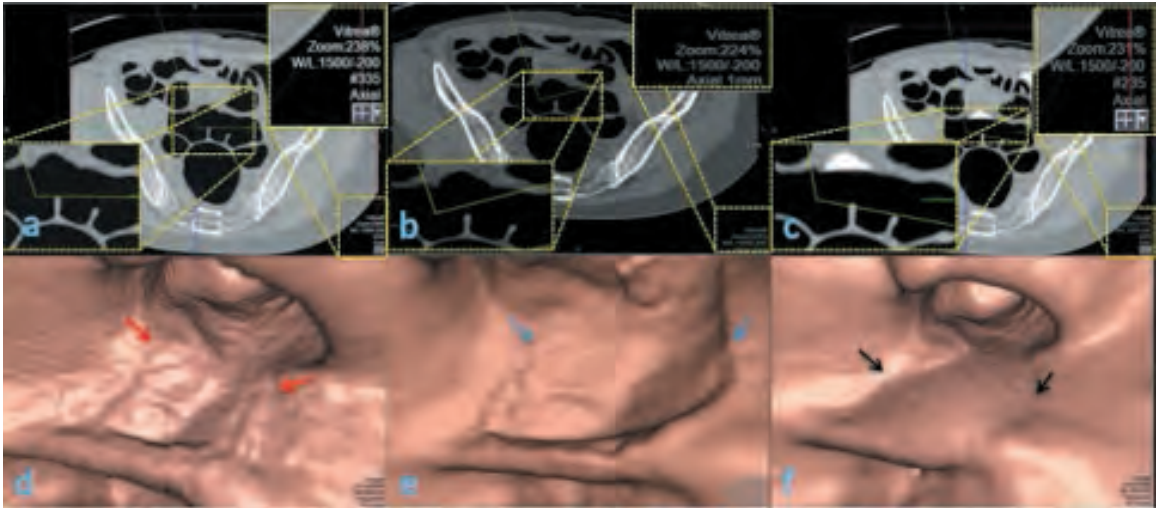


Figure 5.9: Comparison of results of T-junction artifacts removal between the second proposed EC method and EC_{synngo} (a) the axial CTC image of EC result from the second proposed EC method (b) the axial CTC image of EC result from EC_{synngo} (c) the axial CTC image without applying any EC (d) the 3-D band view of (a) (e) the 3-D band view of (b) (f) the 3-D band view of (c)

shows that all submerged folds are preserved. Figure. 5.14 shows that the artifacts at T-junctions are invisible in this case.

For polyp detection in 10 cases (20 scans) from King Chulalongkorn Memorial

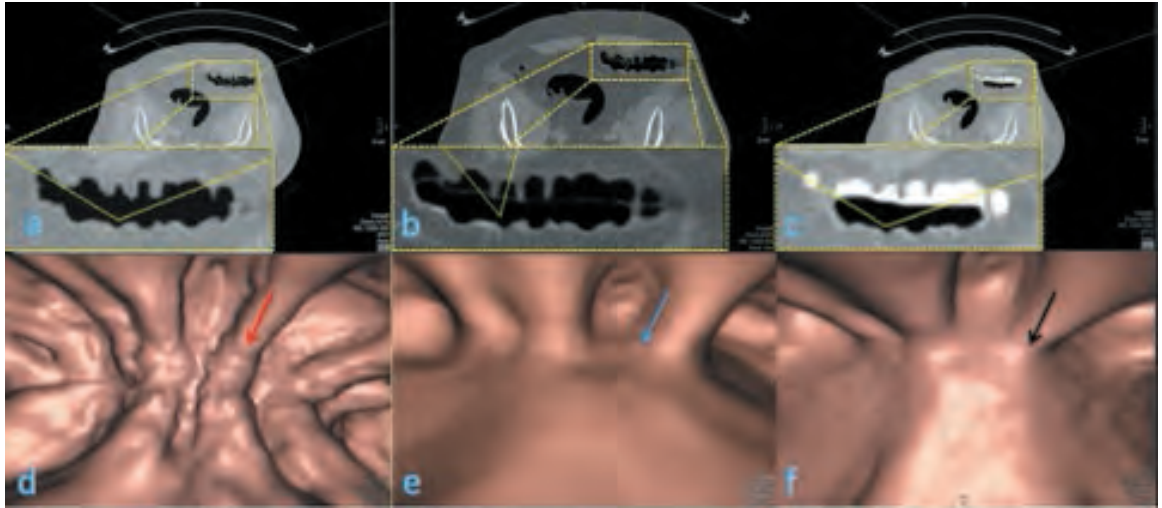


Figure 5.10: Comparison of results of AT or PV effect layer removal between the second proposed EC method and EC_{synngo} (a) the axial CTC image of EC result from the the second proposed EC method (b) the axial CTC image of EC result from EC_{synngo} (c) the axial CTC image without applying any EC (d) the 3-D band view of (a) (e) the 3-D band view of (b) (f) the 3-D band view of (c)

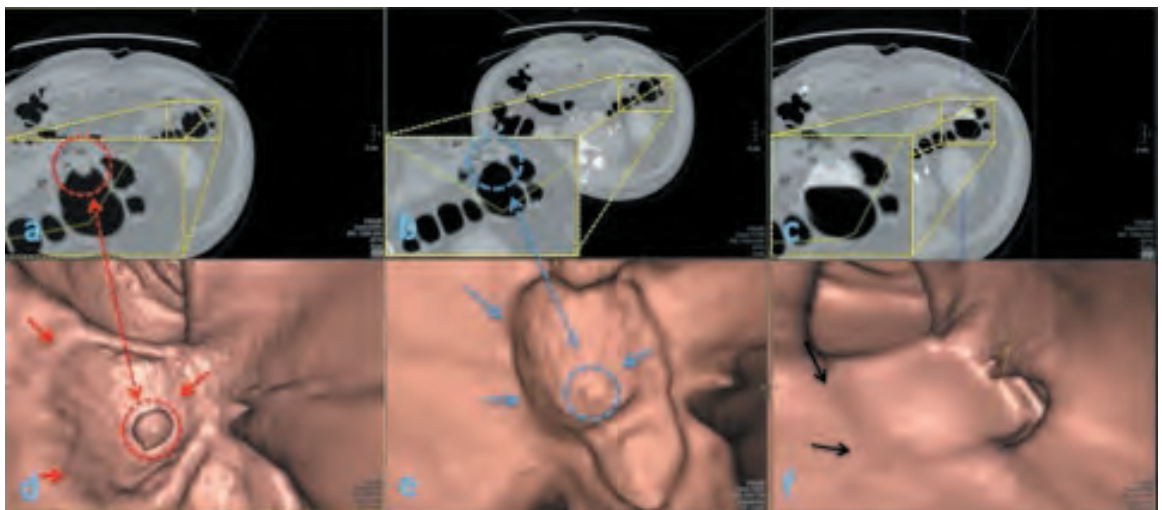


Figure 5.11: Comparison of results of polyp preservation between the second proposed EC method and EC_{synngo} (a) the axial CTC image of EC result from the second proposed EC method (b) the axial CTC image of EC result from EC_{synngo} (c) the axial CTC image without applying any EC (d) the 3-D band view of (a) (e) the 3-D band view of (b) (f) the 3-D band view of (c)

hospital, there are 17 polyps which can be divided into two groups: a group of 12 polyps with size ≥ 6 mm and a group of five polyps with size ≥ 10 mm, respectively. For partially or completely submerged polyps in FTM, there are nine polyps with size ≥ 6 mm and three polyps with size ≥ 10 mm, respectively. All of them are visible in EC_{prop} and EC_{prev} where they could hardly be found in 3-D band view images before applying EC methods. Thus, the sensitivity for polyp detection after EC is as high as 100% (17/17) for both EC_{prop} and EC_{prev} .

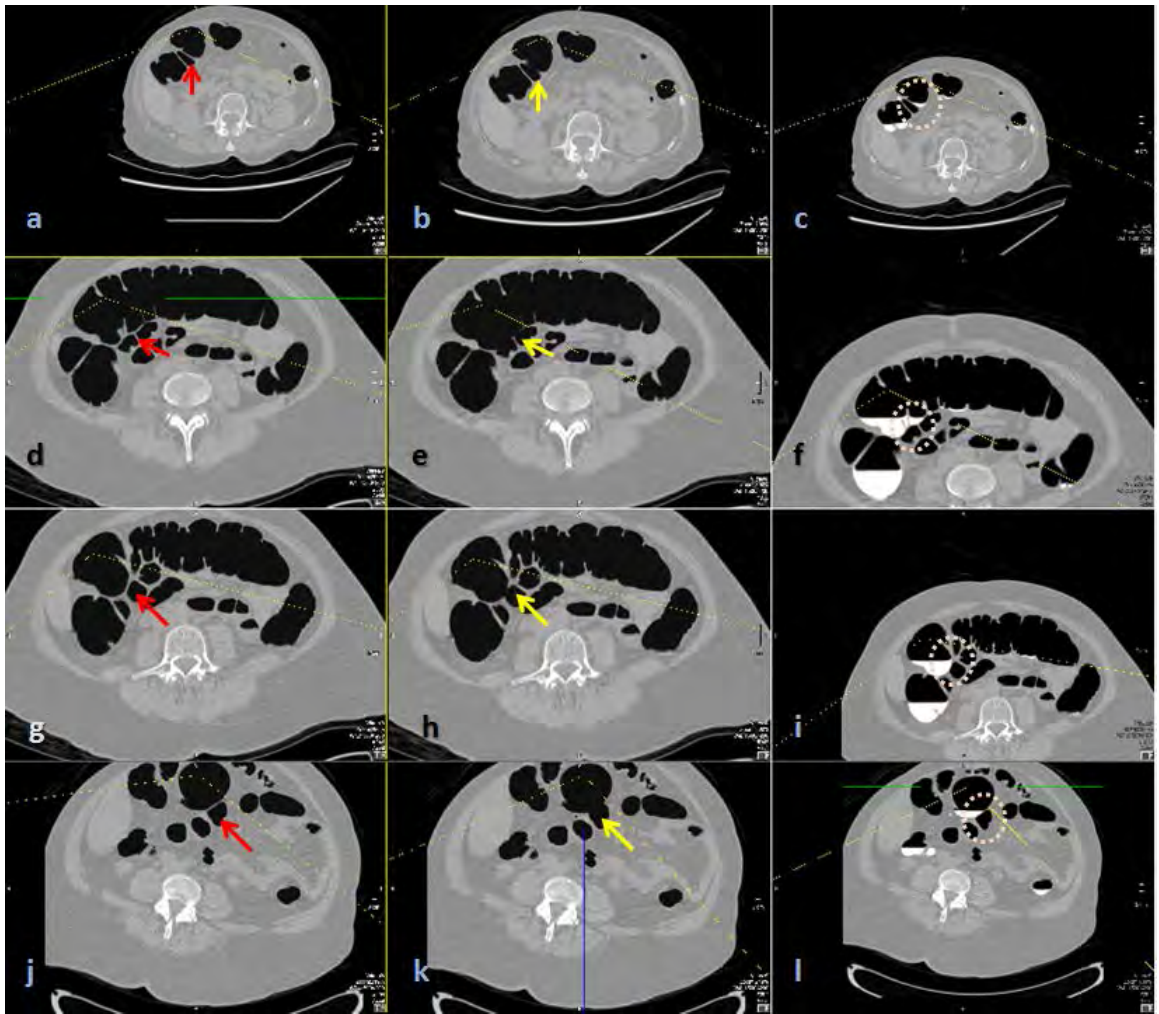


Figure 5.12: Comparison of results of ATT layers preservation between the second proposed EC method, EC_{prop} and the fast three-material model [11], EC_{prev} (a),(d),(g) and (j) are the axial CTC image of EC result from EC_{prop} (b),(e),(h) and (k) are the axial CTC image of EC result from EC_{prev} (c),(f),(i) and (l) are the axial CTC image without applying any EC

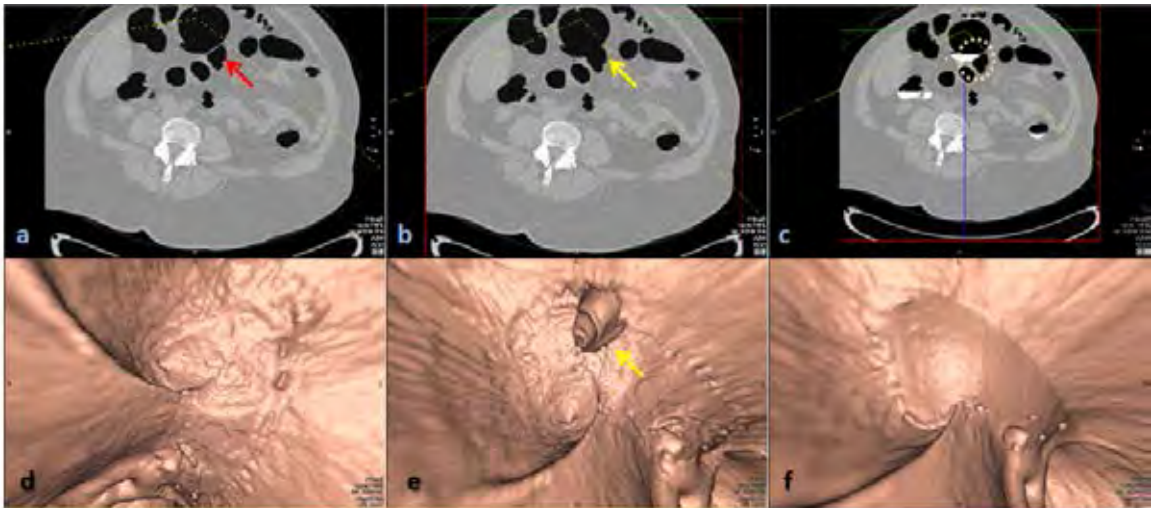


Figure 5.13: Comparison of result of ATT layer preservation in 3-D band view between the second proposed EC, EC_{prop} , and the fast three-material model [11], EC_{prev} (a) the axial CTC image of EC result from EC_{prop} (b) the axial CTC image of EC result from EC_{prev} [11] (c) the axial CTC image without applying any EC (d) the 3-D band view of (a) (e) the 3-D band view of (b) (f) the 3-D band view of (c)

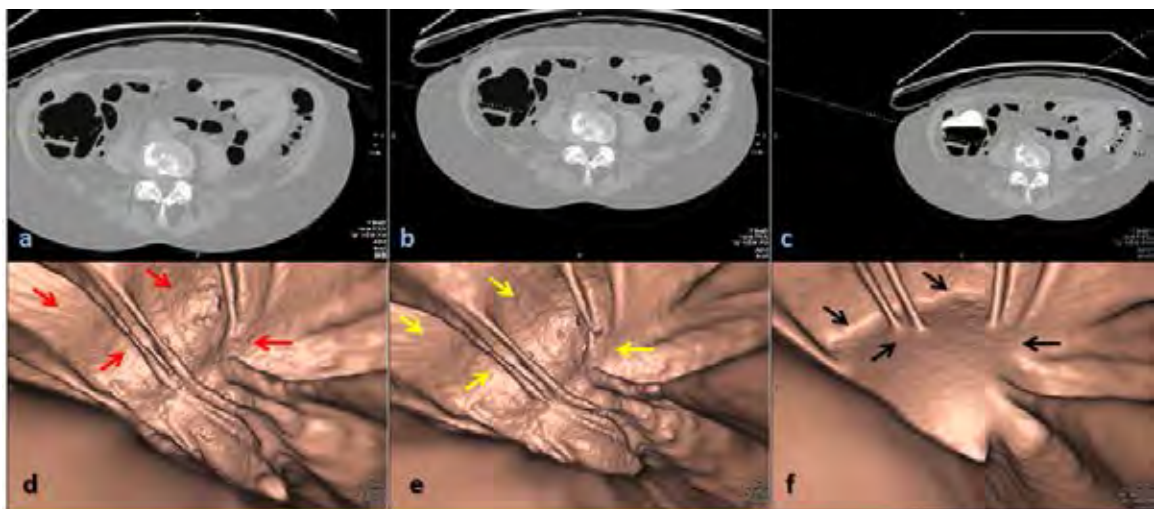


Figure 5.14: Comparison of result of fold preservation in 3-D band view between the second proposed EC, EC_{prop} and the fast three-material model [11], EC_{prev} (a) the axial CTC image of EC result from EC_{prop} (b) the axial CTC image of EC result from EC_{prev} [11] (c) the axial CTC image without applying any EC (d) the 3-D band view of (a) (e) the 3-D band view of (b) (f) the 3-D band view of (c)

CHAPTER VI

DISCUSSION AND CONCLUSION

6.1 Discussion

The first proposed EC method preserve only PEH ST voxels in vicinity of FTM by reducing CT numbers of those voxels without touching FTM voxels while the ADC method [15] reduce CT numbers of FTM voxels and PEH ST voxels around FTM. In order to reduce only PEH ST voxels in vicinity of FTM, the GDSD is used to detect PEH ST voxels in vicinity of FTM. The PEH correction method in the first proposed EC method uses two threshold values to be minimum and maximum values of PEH Soft tissue voxels where these threshold values can be set to cover the possible range of PEH ST CT numbers. The results show that high CT numbers of PEH ST voxels can be reduced to be in the ST range using the proposed PEH correction method. In contrast, the existing ADC method fails to reduce high CT numbers of PEH ST voxels into the ST range. These two threshold values are not suitable for every FTM due to variation of CT numbers in FTM. For the similarity of AT layers and ATT layers, the proposed modified local roughness in the first proposed EC method is used to distinguished AT layers from ATT layers while EC_{prev} [11] does not concern this case. Thus, ATT layers can be preserved from removal after applied the first proposed EC method. Unfortunately, we did not compare the first proposed EC method to any the existing method. However, the first proposed EC method still cannot remove artifacts at T-junctions where air, ST, and FTM meet simultaneously. Thus, the second EC method was proposed.

The second proposed EC method can preserve PEH ST voxels by changing CT numbers of PEH ST voxels into ST CT numbers range with the integration of GDSD and linear combination of three material fractions. The AT layer identification algorithm removes ATT layers from ambiguous layers. The remaining layers after applied the AT

layers identification are AT layers. Then, CT numbers of AT layers, artifacts at T-junction and FTM voxels are changed to CT numbers of air using linear combination of three material fractions. Thus, the ATT layers are preserved after applied the second proposed EC method while while EC_{prev} [11] cannot take care this case. The rut-like structural response in EC_{prev} [11] cannot preserve ATT layers because ATT layer structure is not rut shape.

However, the specificity of polyp detection in the first and second proposed EC method does not exist because the specific location of polyp that was identified in virtual colonoscopy after applied the propose EC methods was not confirmed the location of polyp using OC in this study. The polyp locations after applied the proposed EC methods are only compared with the reference locations of the radiologist in CTC images. Thus, there is only the sensitivity of polyp detection in this study.

6.2 Conclusion

In the conclusion, there are two proposed EC methods to solve the problems of the existing EC which are PEH effect, the similarity of AT and ATT layers and the artifacts at T-junction where AT layers need to be removed while ATT layers need to be preserved.

For the first proposed EC method, it can solve the PEH effect and the similarity between AT and ATT layers. The PEH effect problem is solved by using the GDSD to detect the ST voxels around FTM. After ST voxels are obtained, the linear transformation is used to reduce CT numbers of PEH ST voxels to the standard ST range. Next, the similarity between AT and ATT layers can be distinguished by using the modified local roughness with layer labeling. After AT layers are detected, the FTMs and AT layers are removed by the first proposed EC method.

For the second proposed EC method, the PEH effect can be solved by integrating the GDSD into material fraction model. The ATT layers are preserved by using AT layer identification. After AT layers are identified, ATT layers are spared from EC removal while AT layers are removed using the linear combination equation of three material

fractions which can remove the artifacts at T-junction.

The results of the first proposed EC method are passed through both subjective and objective evaluations. For subjective evaluation, the clinical evaluation was performed in order to assess the cleansing quality. The results of clinical evaluation indicate the reliability of cleansing quality. For objective evaluation, the PEH correction results were compared to those of the existing ADC method. The visual assessment shows that ATT layers are preserved while AT layers are removed without confusing. The results of IFTM case show that it is possible to use the first proposed EC method.

Next, the clinical evaluation is performed on the results of the second proposed EC method. The cleansing quality is measured by the radiologist. The results of cleansing quality show the reliability of the second proposed EC method where the least remaining of artifacts at T-junction cannot be identified by the radiologist. For the 100% remaining of artifacts at T-junctions, the comparison between the results from the second proposed EC method and those of the Syngo Via software show that the results from the second proposed EC method are more preferable. Finally, the comparison between the second proposed EC method and the fast three material fractions are performed. The slight improvement in the second proposed EC method comes from ATT layers preservation while the fast three material fractions fails to preserve them.

References

1. Boyes, R., Slabugh, G., and Beddoe, G. 2009. Fast pseudo-enhancement correction in ct colonography using linear shift-invariant filters. In ICIP, pp. 2509–2512. : IEEE.
2. Cai, W., Zalis, E. M., Näppi, J., Harris, J. G., and Yoshida, H. 2008. Structure-analysis method for electronic cleansing in cathartic and noncathartic ct colonography. Med. Phys. 35.7 (2008): 3259–3277.
3. Callstrom, M. R., Johnson, C. D., Fletcher, J. G., Reed, J. E., Ahlquist, D. A., Harmsen, W. S., Tait, K., Wilson, L. A., and Corcoran, K. E. 2001. Ct colonography without cathartic preparation: Feasibility study. Radiology 219.3 (2001): 693–698.
4. Elwood, J. M., Ali, G., Schlup, M. M., McNoe, B., Barbezat, G. O., North, F., Sutton, K., Parry, B., and Chadwick, V. S. 1995. Flexible sigmoidoscopy or colonoscopy for colorectal screening: A randomized trial of performance and acceptability. Cancer Dtect. Prev. 19.4 (1995): 337–347.
5. Frigo, M. and Johnson, S. G. 2012. fftw version 3.3.3. Tech. Rep and Massachusetts Institute of Technology.
6. Gluecker, T. M., Johnson, C. D., Harmsen, W. S., Offord, K. P., Harris, A. M., Wilson, L. A., and Ahlquist, D. A. 2003. Colorectal cancer screening with ct colonography, colonoscopy, and double-contrast barium enema examination: Prospective assessment of patient perceptions and preferences. Radiology 227.2 (2003): 378–384.
7. Goldman, R. 2005. Curvature formulas for implicit curves and surface. Computer Aided Geometric Design 22 (2005): 632–665.
8. Ho, S., Bullitt, E., and Gerig, G. 2002. Level set evolution with region competition: automatic 3d segmentation of brain tumors. In International Conference on Pattern Recognition. Quebec City, Canada: IEEE.

9. Law, W. K. M. and Chung, C. S. A. 2009. Efficient implementation for spherical flux computation and its application to vascular segmentation. IEEE Trans. Image. Proc. 18.3 (2009): 596–612.
10. Lee, H., Kim, B., Lee, J., Kim, S. H., Shin, Y. G., and Kim, T. G. 2013. Fold-preserving electronic cleansing using a reconstruction model integrating material fractions and structural responses. IEEE Trans. Biomed. Eng. 60.6 (2013): 1546–1555.
11. Lee, H., Lee, J., Kim, B., Kim, S. H., and Shin, Y. G. 2014. Fast three-material modeling with triple arch projection for electronic cleansing in ctc. IEEE Trans. Biomed. Eng. 61.7 (2014): 2102–2111.
12. Liang, Z., Yang, F., Wax, M., Li, J., You, J., Kaufman, A., Hong, L., Li, H., and Viswambharan, A. 1997. Inclusion of a priori information in segmentation of colon lumen for 3d virtual colonoscopy. In IEEE Nuclear Science Society-Medical Imaging Conference. : IEEE.
13. Liang, Z., Chen, D., Chiou, R., Li, B., Kaufman, A., Wax, M., and Viswambharan, A. 1999. On segmentation of colon lumen for virtual colonoscopy. In SPIE Medical Imaging Conference. San Diego: Addison-Wesley publ Reading.
14. Liu, J., Yao, J., and Summers, R. M. 2008. Scale-based scatter correction for computer-aided polyp detection in ct colonography. Med. Phys. 35.12 (2008): 5664–5671.
15. Näppi, J. and Yoshida, H. 2008. Adaptive correction of the pseudo-enhancement of ct attenuation for fecal-tagging ct colonography. Medical Image Analysis 12 (2008): 413–426.
16. Näppi, J. and Yoshida, H. 2007. Fully automated three-dimensional detection of polyps in fecal-tagging ct colonography. Acad. Radiol. 25 (2007): 287–300.
17. Oppenheim, A. V., Schafer, R. W., and Buck, J. W. 1998. Discrete-Time Signal Processing. Prentice Hall Signal Processing Series.

18. Otsu, N. 1979. A threshold selection method from gray level histograms. IEEE trans. Syst. Man Cybern 9 (1979): 6266.
19. Pickhardt, P. J., Choi, J. R., Hwang, I., Butler, J. A., Puckett, L., Hildebrandt, H. A., Wong, R. K., Nugent, P. A., Mysliwiec, P. A., and Schindler, W. R. 2003. Computed tomographic virtual colonoscopy to screen for colorectal neoplasia in asymptomatic adults. N. Engl. J. Med. 349.23 (2003): 2191–2200.
20. Pickhardt, P. J., Hasan, C., Halligan, S., and MarMo, R. 2011. Colorectal cancer: Ct colonography and colonoscopy for detection-systematic review and meta-analysis. Radiology 259 (2011): 393–405.
21. Prokop, M. and Galanski, M. 2005. Spiral and multislice computed tomography of the body. Radiology 236 (2005): 118–124.
22. Ravesteijn, F. v. V., Boellaard, N. T., Paardt, P. v. d. M., Serlie, H. C. d. M., W.O. I., Stoker, J., Vliet, J. v. L., and Vos, M. F. 2013. Electronic cleansing for 24-h limited bowel preparation ct colonography using principal curvature flow. IEEE Trans. Bio. Eng. 60.11 (2013): 3036–3045.
23. Ristvedt, S. L., McFarland, E. G., Weinstock, L. B., and Thyssen, E. P. 2003. Patient preferences for ct colonography, conventional colonoscopy, and bowel preparation. Am. J. Gastroenterol. 98.3 (2003): 578–585.
24. Serlie, I. W. O., Vos, F. M., Truyen, R., Post, F. H., and Vliet, L. J. v. 2007. Classifying ct image data into material fractions by a scale and rotation invariant edge model. IEEE Trans. Imag. Proc. 16.12 (2007): 2891–2904.
25. Serlie, I. W. O., Vos, F. M., Truyen, R., Post, F. H., Stoker, J., and Vliet, L. J. v. 2010. Electronic cleansing for computed tomography (ct) colonography using a scale-invariant three material model. IEEE Trans. Biomed. Eng. 57.6 (2010): 1306–1317.
26. Society, A. C. 2004. Cancer facts and figures. American Cancer Society.
27. Timothy, G. 2010. The Mathematics of Medical Imaging: A Beginner’s Guide. Springer Undergraduate Texts in Mathematics and Technology.

28. Tsagaan, B., Näppi, J., and Yoshida, H. 2009. Nonlinear regression-based method for pseudoenhancement correction in ct colonography. Med. Phys. 36.8 (2009): 3596–3606.
29. Wardle, J., Sutton, S., Williamson, S., Taylor, T., McCaffery, K., Cuzick, J., Hart, A., and Atkin, W. 2000. Psychosocial influences on older adults' interest in participating in bowel cancer screening. Prev. Med. 31.4 (2000): 323–334.
30. Weitzman, E. R., Zapka, J., Estabrook, B., and Goins, K. V. 2001. Risk and reluctance: Understanding impediments to colorectal cancer screening. Prev. Med. 32.6 (2001): 502–513.
31. Zalis, M., Perumpillichira, J., Kim, J., Del Frate, C., Magee, C., and Hahn, P. 2005. Polyp size at ct colonography after electronic subtraction cleansing in an anthropomorphic colon phantom. Radiology 236 (2005): 118–124.
32. Zalis, M. E. and Hahn, P. F. 2001. Digital subtraction bowel cleansing in ct colonoscopy. AJR, Am. J. Roentgenol 176.3 (2001): 646–648.
33. Zalis, M. E., Perumpilichira, J., and Hahn, P. F. 2004. Digital subtraction bowel cleansing for ct colonography using morphological and linear filtration methods. IEEE trans. Med. Imaging 23.11 (2004): 1335–1343.
34. Zalis, M. E., Blake, M. A., Cai, W., Hahn, P. F., Halpern, E. F., Kazam, I. G., Keroack, M., Magee, C., Näppi, J., Perez-Johnston, R., Saltzman, J. R., Vij, A., Yee, J., and Yoshida, H. 2012. Diagnostic accuracy of laxative-free computed tomographic colonography for detection of adenomatous polyps in asymptomatic adults. Ann Intern Med. 156 (2012): 692–702.

APPENDICES

APPENDIX A : Boundary evaluation

In this section, the evaluation on voxels in the vicinity of FTM is used in order to measure the goodness of cleansing instead of the goodness of cleansing in the previous. Because the previous goodness of cleansing includes all area of FTM in a ROI but the goodness of cleansing results are different from the ground truth only around the vicinity of FTM. Thus, it is more reasonable to measure the goodness of cleansing only in vicinity of FTM.

The boundary binary image of the ground truth in Fig. 1(c) is used to find the vicinity of FTM where Fig. 1(b) is a example of ground truth Fig. 1(b) is the area of FTM in Fig. 1(a). The boundary binary image in Fig. 1(d) is a example of the results of Fig. 1(a).

In order to measure the goodness of cleansing only in vicinity of FTM, the boundary binary image of Fig. 1(c) are dilated with four sizes of square structure element where

- Fig. 2(a) is dilated with square structure element of size 2,
- Fig. 2(b) is dilated with square structure element of size 3,
- Fig. 2(c) is dilated with square structure element of size 4, and
- Fig. 2(d) is dilated with square structure element of size 5.

The boundary binary image of result is dilated with four sizes either where case 1 is the boundary binary image of the result of the first proposed EC method and case 2,3, and 4 are dilated with square structure element of size 2, 3, and 4, respectively. To compare the difference between the vicinity of FTM in ground truth and result, the exclusive-OR operation (XOR) is used. However, the square structure element of size 5 is too wide. Thus, it is not used in this evaluation.

Without applying the dilation operation, the number of voxel in boundary of the result of the first proposed EC method is 99194 and the number of voxel in boundary of

the ground truth is 116687. In table. 1, there is only numbers on the upper triangle of the table because they are used to indicate the number of difference between the boundary voxels of result from the ground truth and the first proposed EC method when the square structure element size of the ground truth is higher than those of the first proposed EC method.

The percentage of the second column is equal to or high because the boundary binary image of ground truth and the boundary binary image of result are not in the same position in every single FTM object. The last column is getting lower and lower for applying higher size of square structure element in both ground truth and result. For the size of structure element, it is not surprised if the XOR result is low after applying the dilation with high size of square structure element. Although the low of difference from applying the dilation with high size of square structure element does not indicate the goodness of cleansing but it should have the acceptable size of structure element which can indicate the goodness of cleansing. We found that if size of square structure element is 3, the XOR result can be low too as shown in the fourth column and third row in Table. 1. Thus, the difference between the boundary binary image of the ground truth with square structure element of size 3 in dilation operation and the boundary binary image of the first proposed EC method with square structure element of size 3 in dilation operation is 35.37% using XOR operation.

Table 1: XOR result between ground truth and result of the first proposed EC method

case/size	1	2	3	4
1	103%	83.47%	75.45%	81.15%
2	-	79.27%	40.81%	51.50%
3	-	-	35.37%	39.17%
4	-	-	-	39.37%

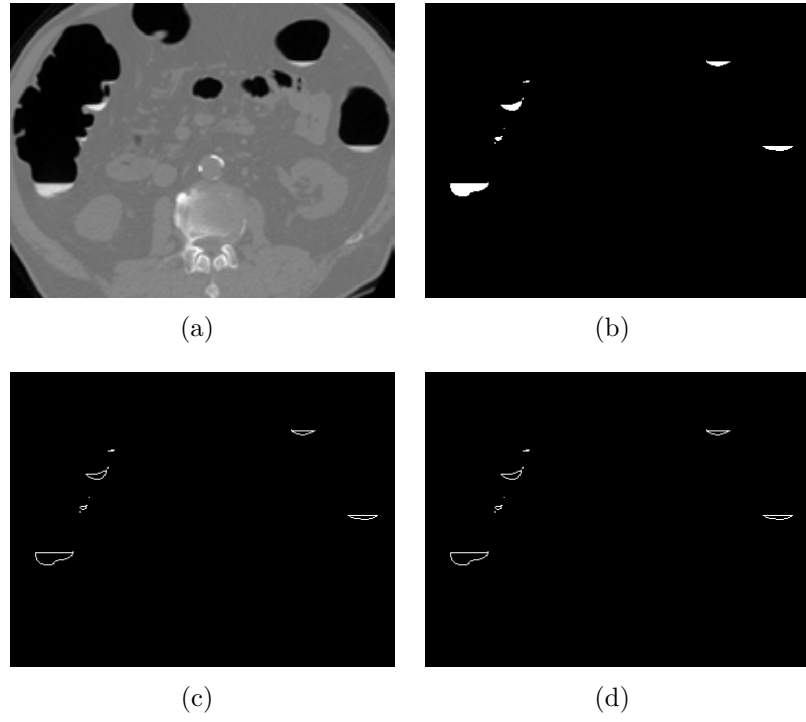


Figure 1: (a) a CTC image (b) ground truth (c) boundary of the ground truth (d) boundary of the first proposed EC result

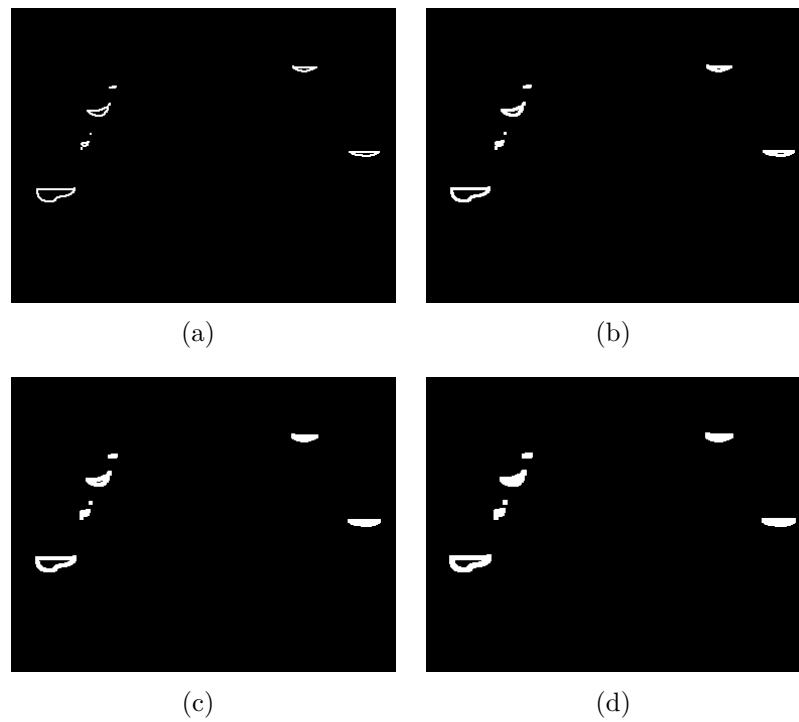


Figure 2: (a) Dilation of Fig. 1(c) with square element structure element size 2 (b) Dilation of Fig. 1(c) with square element structure element size 3 (c) Dilation of Fig. 1(c) with square element structure element size 4 (d) Dilation of Fig. 1(c) with square element structure element size 5

APPENDIX B : Ethical consideration and King Chulalongkorn Memorial Hospital permission

This research is an experimental study. Ethical consideration has been processed and approved in October 2015 by the ethic committee, Faculty of Medicine Chulalongkorn University as follows:



COA No. 725/2015

IRB No. 359/58

INSTITUTIONAL REVIEW BOARD

Faculty of Medicine, Chulalongkorn University

1873 Rama 4 Road, Patumwan, Bangkok 10330, Thailand, Tel 662-256-4493 ext 14, 15

Certificate of Approval

The Institutional Review Board of the Faculty of Medicine, Chulalongkorn University, Bangkok, Thailand, has approved the following study which is to be carried out in compliance with the International guidelines for human research protection as Declaration of Helsinki, The Belmont Report, CIOMS Guideline and International Conference on Harmonization in Good Clinical Practice (ICH-GCP)

Study Title : Electronic Cleansing and Polyp Detection in CT Colonography images

Study Code : -

Principal Investigator : Mr. Krisorn Chunhapongpipat

Affiliation of PI : Faculty of Science, Chulalongkorn University.

Review Method : Expedited

Continuing Report : At least once annually or submit the final report if finished.

Document Reviewed :

1. Research Proposal Version 1.0 Date 29 September 2015
2. Protocol Synopsis Version 1.0 Date 1 July 2015
3. CRF Form
4. Principal investigator's CV
5. GCP Training

Signature: 

(Emeritus Professor Tada Sueblinvong MD)

Chairperson

The Institutional Review Board

Signature: 

(Assistant Professor Prapapan Rajatapiti MD, PhD)

Member and Secretary

Secretary The Institutional Review Board

Date of Approval : October 15, 2015

Approval Expire Date : October 14, 2016

Approval granted is subject to the following conditions: (see back of this Certificate)

All approved investigators must comply with the following conditions:

1. Strictly conduct the research as required by the protocol;
2. Use only the information sheet, consent form (and recruitment materials, if any), interview outlines and/or questionnaires bearing the Institutional Review Board's seal of approval ; and return one copy of such documents of the first subject recruited to the Institutional Review Board (IRB) for the record;
3. Report to the Institutional Review Board any serious adverse event or any changes in the research activity within five working days;
4. Provide reports to the Institutional Review Board concerning the progress of the research upon the specified period of time or when requested;
5. If the study cannot be finished within the expire date of the approval certificate, the investigator is obliged to reapply for approval at least one month before the date of expiration.
6. If the research project is completed, the researcher must be form the Faculty of Medicine, Chulalongkorn University.

* A list of the Institutional Review Board members (names and positions) present at the meeting of Institutional Review Board on the date of approval of this study has been attached. All approved documents will be forwarded to the principal investigator.

ที่ จพ.รต. 5507 / 2558



โรงพยาบาลจุฬาลงกรณ์
1873 ถนนพระรามที่ 4
แขวงปทุมวัน เขตปทุมวัน
กรุงเทพฯ 10330

16 ธันวาคม 2558

เรื่อง การขอใช้ข้อมูลภาพ CT Colonography
เรียน ศาสตราจารย์ ดร.ชิตชนก เหลือสินทรัพย์
อ้างถึง หนังสือที่ กณ 1384 / 2558 ลงวันที่ 30 กันยายน 2558

ตามหนังสือที่อ้างถึง ภาควิชาคณิตศาสตร์และวิทยาการคอมพิวเตอร์ คณะวิทยาศาสตร์ - จุฬาลงกรณ์มหาวิทยาลัย แจ้งว่า นายไกรสร ชูณพงษ์พิพัฒน์ นิสิตระดับวิทยาศาสตร์ดุสิตบัณฑิต สาขาวิชาวิทยาการคอมพิวเตอร์และเทคโนโลยีสารสนเทศ ได้จัดทำวิจัยเพื่อเสนอเป็นวิทยานิพนธ์ เรื่อง " การล้างลำไส้ใหญ่และการตรวจหาโพลีพอด โนมิตแบบสามมิติใช้วิธีการร่วมมือของสนามการไหลเวกเตอร์ ในเซตระดับ " และในการนี้ ได้ขออนุญาตใช้ข้อมูลภาพ CT Colonography ของผู้ป่วยในงานวิจัย ณ ฝ่าย - รังสีวิทยา โรงพยาบาลจุฬาลงกรณ์ ดังรายละเอียดแจ้งแล้ว นั้น

โรงพยาบาลจุฬาลงกรณ์พิจารณาแล้ว ไม่ขัดข้อง ยินดีให้ดำเนินการตามที่ขอมาโดยติดต่อ ประสานงานได้ที่ ฝ่ายรังสีวิทยา โทรศัพท์ 02-256-4412 อนึ่ง ก่อนเข้าพบบุคคลดังกล่าวขอให้นำบัตร นักศึกษาหรือบัตรประจำตัวประชาชนพร้อมจดหมายฉบับนี้ มาติดต่อขอรับบัตรประจำตัวผู้เก็บข้อมูล ณ ฝ่าย - เลขานุการ ตึกอำนวยการ ชั้นล่าง ห้องหมายเลข 2

จึงเรียนมาเพื่อทราบ

ขอแสดงความนับถือ

(ศาสตราจารย์นายแพทย์สุเทพ กลชาญวิทย์)

รองผู้อำนวยการฯ ฝ่ายการแพทย์และวิจัย

ปฏิบัติการแทน ผู้อำนวยการ โรงพยาบาลจุฬาลงกรณ์

กลุ่มงานร่างได้คอบเอกสาร ฝ่ายเลขานุการ ติดต่อประสานงาน : สุกัญญา โทรศัพท์ : 0-2256-4312 / โทรสาร : 0-2256-4368

APPENDIX C :List of Abbreviations

Table 2: List of abbreviations

Abbreviation	Terms
3D	3 dimensions
ADC	The adaptive density-correction method
AT layer	artifact interface layer between air and fecal-tagging material
ATT layer	thin soft tissue layer between air and fecal-tagging material
CTC	Computed tomography colonography
DBC	digital bowel cleansing
EC	electronic cleansing
ECC	electronic colon cleansing
EC_{prev}	The fast three-material model [11]
EC_{prop}	The second proposed EC method
EC_{syngo}	the syngo.via client 3.0 software of Siemen CT scanner
FTM	fecal-tagging material
GDS	gradient directional second derivative
HU	Hounsfield unit
OC	optical colonoscopy
PEH	pseudo-enhancement
PV effect	partial volume effect
ROI	region of interest
SEER	Surveillance, Epidemiology, and End result summary staging system
ST	soft-tissue
STT layer	boundary between ST and FTM
T-junction	junction of three materials where air, soft tissue and fecal-tagging material meet simultaneously
TNM	Tumor, Node, Metastasis system
VOI	volume of interest
XOR operation	exclusive-OR operation

Biography

Name	Mr. Krisorn Chunhapongpipat
Date of Birth	2 August 1984
Place of Birth	Bangkok, Thailand
Education	B.Sc. (2006) and M.Sc. (2010) in computer science and information technology, Chulalongkorn University
Scholarship	THE 90th ANNIVERSARY OF CHULALONGKORN UNIVERSITY SCHOLARSHIPS and CENTRE OF EXCELLENCE IN MATHEMATICS SCHOLARSHIPS FROM MAHIDOL UNIVERSITY.
Publication	<ul style="list-style-type: none"> • <i>Automatic Colon Cleansing in CTC Image Using Gradient Magnitude and Similarity Measure</i>, Krisorn Chunhapongpipat, Laddawan Vajragupta, Bundit Chaopathomkul, Nagul Cooharajanane, and Rajalida Lipikorn, the 6th International Conference, SIP 2009, Jeju Island, Korea, December 2009. • <i>Medical Image Segmentation Using Modified Level-Set Model with Multi-Scale Gradients Vector Flow</i>, Rajalida Lipikorn, Krisorn Chunhapongpipat, Sirod Sirisup, Ratinun Boonklurb, and Nagul Cooharajanane, International Symposium on Signal Processing, Image Processing and Pattern Recognition, Vol. 123, pp.49-57, December 2010. • <i>Edge and Contrast Enhancement using Directional Anisotropic Diffusion and Multi-Scale Vector Flows</i>, Krisorn Chunhapongpipat, Ratinan Boonklurb, Rajalida Lipikorn, and Sirod Sirisup, IASTED Conferences Signal and Image Processing, SIP 2012, Honolulu, USA, August 2012. • <i>Initial Contour Independent Level Set Image Segmentation Method using Synergetic Vector Flow Fields</i>, Krisorn Chunhapongpipat, Ratinan Boonklurb, Rajalida Lipikorn, and Sirod Sirisup, Signal Processing and Communication Systems (ICSPCS), Gold Coast, Australia, December 2012.